Earth, Planets and Space

FULL PAPER Open Access

Stress field in northeastern Japan and its relationship with faults of recent earthquakes

Ayaka Tagami[1*], Miu Matsuno[1], Tomomi Okada[1], Shin'ichi Sakai[2], Mako Ohzono[3], Kei Katsumata[3], Masahiro Kosuga[4], Yoshiko Yamanaka[5], Hiroshi Katao[6], Takeshi Matsushima[7], Hiroshi Yakiwara[8], Satoshi Hirahara[1], Toshio Kono[1], Shu'ichiro Hori[1], Toru Matsuzawa[1], Shuutoku Kimura[1], Takashi Nakayama[9] and Group for the aftershock observations of the 2011 off the Pacific coast of Tohoku Earthquake

Abstract

Inversion tectonics, in which old normal faults act as reverse faults in current stress fields, are frequently observed in northeastern Japan (Tohoku District); however, the conditions that control these fault activities remain unclear. To improve the identification of faults that are more favorable to slip under current stress conditions, the regional fault mechanisms in the Tohoku District must be better understood. The stress field in the Tohoku District and the likelihood of fault activities were thus estimated using slip tendency (ST) analysis. The results show that in the eastern margin of the Japan Sea (EMJS), the reverse fault type is dominant in the stress field. The maximum horizontal direction changes clockwise from E–W to NW–SE from the northern to the southern regions and counterclockwise from NW–SE to E–W from the Japan Sea to the inland area. In the Tohoku inland area, the estimated direction of the maximum horizontal axis changed after the 2011 Tohoku-Oki earthquake, from E–W to WNW–ESE. ST values were calculated for seven events in the EMJS area. To avoid the influence of the Tohoku-Oki earthquake, only stress field data prior to the 2011 Tohoku-Oki earthquake were used to determine ST values for four of the events in the Tohoku inland area. The results showed eastward-dipping fault planes with low dip angles (approximately 30°–45°) and large ST values (approximately > 0.7). The large ST values indicate that the stress field fault is favorable to slip and the results were consistent with the actual fault plane in the EMJS area. However, in the Tohoku inland area and the southern part of fault model of the 1993 Hokkaido Nansei-Oki earthquake, fault planes with large ST values were found to be inconsistent with the slipped fault plane, thus indicating that slipping was unfavorable. The regional differences are consistent with the volcano distribution and thus, the fluid supply from volcanic activity may have helped the fault slip under difficult stress conditions.

Keywords Fault activity, Stress field, Slip tendency analysis, Northeastern Japan, Inversion tectonics

*Correspondence:
Ayaka Tagami
ayaka.tagami.p6@dc.tohoku.ac.jp
Full list of author information is available at the end of the article

Graphical Abstract

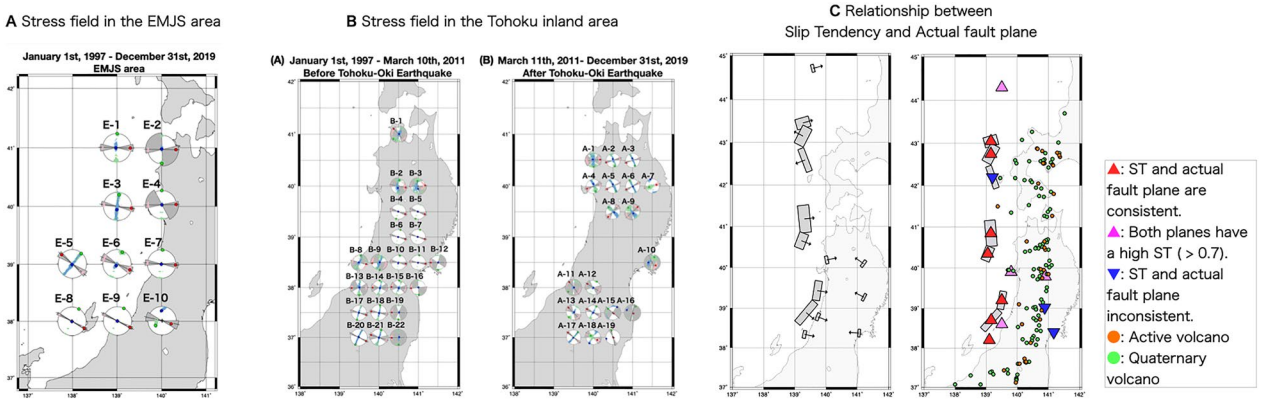

Introduction

In the region of northeastern Japan (Fig. 1A), the Pacific Plate subducts to the main island of Japan, and converges in an east–west direction. In the eastern margin of the Japan Sea (EMJS; Fig. 1A), due to the eastward movement of the Amur Plate relative to the Pacific Plate, a primary subduction zone has begun to form (e.g., Taira 2001). In the Tohoku region of Japan, stress fields with reverse fault types and east–west compressional axes are thus widely distributed (e.g., Terakawa and Matsu'ura 2010, 2023). The current compressional stress fields are estimated to have begun approximately three million years ago during the Quaternary period (e.g., Sato 1994; Taira 2001).

Several large earthquakes have occurred in the EMJS from Hokkaido to Niigata (e.g., Okamura 2010; Fig. 1A). Strain has been released from several faults and folds distributed in the north–south direction of the EMJS (e.g., Earthquake Research Committee 2003; see examples in Fig. 1B); these faults and folds are subsequently referred to as strain-concentrated zones (intense deformation zones in the EMJS; e.g., Okamura and Kato 2002) and defined as primary subduction zones (e.g., Kobayashi 1983). Faults in the EMJS area are thought to have been formed due to the interactions of a tensional stress field associated with the formation of the Japan Sea (e.g., Jolivet et al. 1994; Okamura 2010). Consequently, numerous high-dip-angle fault planes are widely distributed in the EMJS and Tohoku Districts of Japan (Okamura and Kato 2002; Okamura 2010). Current compressive stress fields cause fault activity in this area; however, the fault activity is strongly controlled by old geological structures formed during the formation of the Japan Sea. Inversion tectonics, in which old normal faults (high-dip-angle fault planes) now dip westward and act as reverse faults, are believed to be existent (Okamura et al. 1995). In the inland area of the Tohoku District, some recent large earthquakes have occurred on the high dip angle with westward-dipping fault plane (e.g., the 1998 Shizukuishi earthquake [M_{jma} 6.1; Umino et al. 1998], 2003 northern Miyagi earthquake [M_{jma} 6.4; Okada et al. 2003; Yoshida et al. 2016], and 2008 Iwate-Miyagi Nairiku earthquake [M_{jma} 7.2; Okada et al. 2012; Yoshida et al. 2014]; Fig. 1A), which may correspond to the eastern boundary of the contraction and uplifting of the Tohoku backbone range (e.g., Okada et al. 2010). However, recent large earthquakes (e.g., the 1940 Shakotan-Oki earthquake [M_{jma} 7.5], 1964 Niigata earthquake [M_{jma} 7.5], and 2019 Yamagata-Oki earthquake [M_{jma} 6.7]) are confirmed to have occurred on low dip angle with eastward-dipping fault plane, and this may be related to eastward incipient subduction of the oceanic lithosphere along the EMJS (Fukao and Furumoto 1975; Satake 1983; Hurukawa and Harada 2013; Earthquake Research Committee 2019; Fig. 1A).

Based on the given data, the following two possibilities exist for fault activity in Tohoku, Japan: (1) inversion tectonics, in which an old normal fault plane with a high dip angle (approximately $45° - 60°$) acts as a reverse fault, or (2) a reverse fault with a low dip angle (approximately $30° - 45°$) was formed in the present stress field.

The activated fault planes in large earthquakes that have occurred in the Tohoku District of Japan, including the EMJS area have been studied using aftershock distribution, tsunami source models, and reflection surveys (e.g., Satake 1986; Okamura et al. 1998; Tanioka et al. 1995; Yoshida et al. 2014; Sibson 2009). Sibson (2009) summarized the inland earthquakes that have occurred since 1896; some of these may have been unfavorably oriented faults under the assumption of the Andersonian faulting theory, in which one of the principal axes of the stress field was coaxial with the fault strike, with σ_3 (minimum principal stress axes)

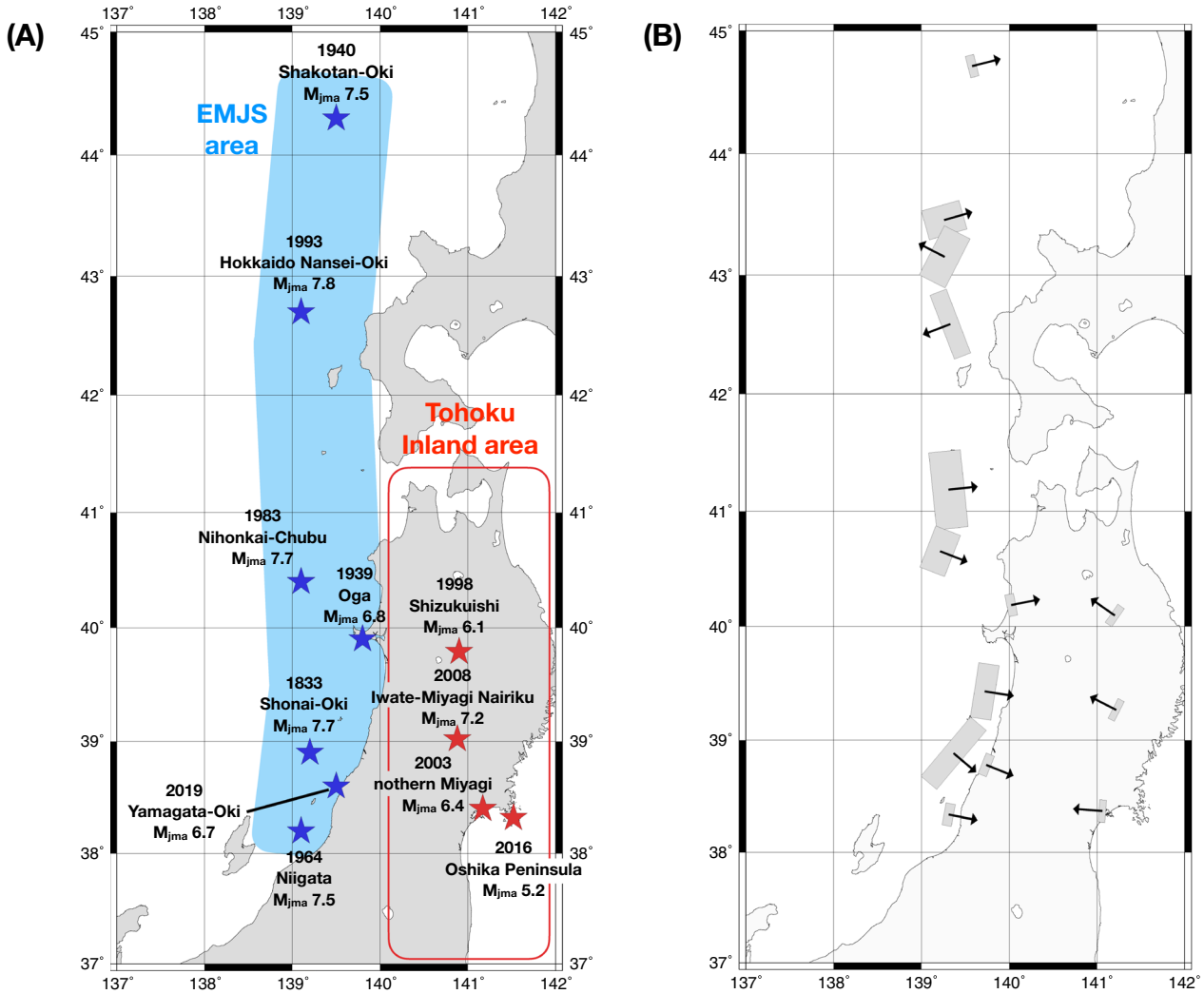

Fig. 1 Study area in the northeastern Japan. In **A**, the blue area denotes the eastern margin of the Japan Sea (EMJS) and the red rectangle identifies the Tohoku District inland area. The blue and red stars indicate the epicenters of the target events in this study, which occurred in the EMJS area and Tohoku District, respectively. **B** The actual fault plane which was estimated in previous studies. The arrows on the fault plane denote the dipping directions

being vertical. However, recent studies (e.g., Terakawa and Matsu'ura 2010, 2023) have shown the heterogeneity of the stress field in northeastern Japan and indicated that fault activities must be evaluated by considering the stress field in each focal area. Other studies have evaluated fault activity by physical methods including the slip tendency (ST) method (Morris et al. 1996). The ST value (Ts) is the ratio of shear stress to normal stress on the fault plane, and can be expressed as follows:

$$Ts = \frac{|\sigma_s|}{\mu|\sigma_n|}, \tag{1}$$

where Ts is the ST value, σ_s shear stress on the fault, σ_n normal stress on the fault, and μ coefficient of the friction on the fault. Ts was normalized between 0 and 1. When Ts is large, the shear stress on the frictional resistance of the fault is also high, thus making it easier for the fault to slip into a stress field.

Yukutake et al. (2015) investigated the applicability of the frictional reactivation theory to faults in Japan and found that faults adequately oriented to the stress fields had high slip ratios (> 1.0 m /1000 years) and large ST values ($Ts > 0.7$). Miyakawa and Otsubo (2015) evaluated ST values using the active fault database of Japan (National Institute of Advanced Industrial Science and Technology) for fault models and found that active faults in the Tohoku region generally had large ST values ($Ts > 0.7$). Furthermore, inactive faults that did not slip during the Quaternary period showed low

ST values ($Ts < 0.6$) (e.g., Miyakawa and Otsubo 2017). However, some active faults (e.g., the Haramachi segment in eastern Fukushima) showed low ST values ($Ts \sim 0.20$), thought to be caused by differences in the dip angle.

Collettini and Trippetta (2007) used the ST method to investigate the relationship between aftershock sequences and the frictional reactivation theory in Colfiorito, Italy, and the 1999 Chi-Chi earthquake (Taiwan). A higher number of aftershocks were found to occur on fault planes with possible slip ($0.6 < Ts < 0.9$) than on the optimal fault plane ($Ts = 1$). Further, they found fewer optimal fault planes in this region, meaning that stress release was performed on other planes.

Moeck et al. (2009) evaluated the reactivation of fractures in geothermal and hydrocarbon reservoir areas using the ST method in the northeast German Basin, and found that the fault system in the volcanic rock layer had a maximum ST value of $Ts = 0.39$, thus it was not optimally oriented to slip. However, experiments with cyclic fluid injections confirmed that microseismicity occurred in the volcanic rock layer, suggesting that even with a small Ts (i.e., the fault is unfavorable for slipping in the stress field), the fault may be active owing to the increased fluid pressure.

In this study, the likelihood of fault activity in the Tohoku District of Japan was estimated using the ST method and the nodal plane of the focal mechanism for the fault model of the previous earthquake. This is the first comprehensive evaluation of the ST method using the nodal planes of the focal mechanisms of actual earthquakes in the Tohoku region. Notably, for the EMJS area and the Tohoku District of Japan, this study tests the hypothesis whether inversion tectonics faults (high dip angle fault plane) or new reverse faults (low dip angle fault plane) are more favorable to slip under the present stress fields, and evaluates the conditions required for fault slip.

Previous studies have estimated the stress field in the EMJS area and Tohoku Districts of Japan. Stress fields were estimated using a small amount of focal mechanism data for the EMJS (Terakawa and Matsu'ura 2010, 2023) or by defining a uniform stress field over a wide area (e.g., Miyakawa and Otsubo 2015). To comprehensively consider the stress state on the fault plane, it was required to evaluate smaller, more localized areas focusing on each earthquake event and/or fault plane, particularly in the EMJS area. The stress field for each earthquake focal area was thus, re-estimated in this study using data from a broader time window that has not been considered in previous studies. The relationship between the obtained ST values, re-estimated stress field, and surrounding environment is then discussed.

Data and methods

Stress fields were calculated using the stress-tensor inversion method developed by Michael (1984, 1987). Michael's method assumes the following three conditions: (1) the same stress tensor acts on the target area; (2) earthquakes occur on existing faults in various directions; and (3) the slip vector direction is equal to shear stress direction on the fault (Wallace–Bott hypothesis). The method statistically estimates the stress field from the nodal plane for the focal mechanisms. One of the nodal planes for the focal mechanisms indicates the actual fault plane. However, as the actual fault plane is unknown in many cases, this method randomly selects the nodal plane and estimates the uncertainties of the principal axes and the stress ratio evaluated using bootstrap resampling (Michael 1987). The method also requires at least eight focal mechanisms to estimate the stress field, and generally, the more data used for the stress-tensor inversion, the more stable the solution will be.

In this study, two focal mechanism catalogs were used to calculate the stress field. The F-net Moment Tensor data (Fukuyama et al. 1998) given by NIED (National Research Institute for Earth Science and Disaster Resilience) were predominantly used. We also used focal mechanism data provided by Okada et al. (2015, 2022) for the inland area of the Tohoku District. Okada et al. (2015, 2022) estimated focal mechanisms using P-wave initial motions from temporary and permanent stations by adopting the method of the Hash program (Hardebeck and Shearer 2002). The Hash program evaluates the quality of focal mechanism based on the relationship between the best fitting solution and the possible solution, misfit of polarity, and station distribution. Only good quality data (quality A or B) from Okada et al. (2015, 2022) were used in this study. If there were duplicate events from both databases, the quality of the F-net moment tensor solution was also evaluated, and if its solution variance reduction was >60, the F-net moment tensor solution was used in the stress inversion. Based on the brittle–ductile transition (e.g., Scholz 1988) and aftershock distribution of large-to-moderate size earthquakes in this area (e.g., Tanioka et al. 1995; Okada et al. 2003; Hurukawa and Harada 2013), earthquakes due to fault activities are presumed to occur at depths of approximately 0–30 km, hence this depth range was used in the present study.

Fault activity was evaluated using the ST method (Morris et al. 1996). The ST value is the ratio of shear stress to normal stress on the fault plane, expressed

Table 1 Slip tendency (ST) for Eastern margin of the Japan Sea (EMJS) calculated using focal mechanism

Event	Fault model	Dip direction	Stress field	*Ts* best	*Ts* error
Shakotan-Oki earthquake	Fukao and Furumoto (1995)	East	1	**0.953**	$0.944 < Ts < 0.993$
	Satake (1986)	West		**0.759**	$0.673 < Ts < 0.915$
Hokkaido Nansei-Oki earthquake	Tanioka et al. (1995) MTRF	East	2—All	0.601	$0.597 < Ts < 0.613$
		West		**0.965**	$0.965 < Ts < 0.975$
		East	2—North	0.619	$0.612 < Ts < 0.645$
		West		**0.976**	$0.975 < Ts < 0.991$
		East	2—South	0.611	$0.603 < Ts < 0.637$
		West		**0.950**	$0.950 < Ts < 0.964$
	Tanioka et al. (1995) CMT	East	2—All	**0.947**	$0.943 < Ts < 0.960$
		West		0.431	$0.412 < Ts < 0.488$
		East	2—North	**0.815**	$0.787 < Ts < 0.996$
		West		0.371	$0.370 < Ts < 0.374$
		East	2—South	**0.955**	$0.953 < Ts < 0.964$
		West		0.440	$0.409 < Ts < 0.531$
Nihonkai-Chubu earthquake	Satake (1985)	East	3—North	**0.915**	$0.914 < Ts < 0.934$
		West		0.429	$0.424 < Ts < 0.443$
		East	3—Middle	**0.850**	$0.836 < Ts < 0.975$
		West		0.506	$0.503 < Ts < 0.514$
		East	3—South	**0.934**	$0.908 < Ts < 0.994$
		West		0.609	$0.601 < Ts < 0.622$
Oga earthquake	Sato (1993)	East	4	**0.914**	$0.902 < Ts < 0.930$
		West		**0.805**	$0.833 < Ts < 0.805$
Niigata earthquake	Hirasawa (1965)	East	6	**0.944**	$0.944 < Ts < 0.971$
		West		0.691	$0.660 < Ts < 0.782$
Yamagata-Oki earthquake	F-net	East	7	**0.905**	$0.905 < Ts < 0.906$
		West		**0.805**	$0.833 < Ts < 0.805$

ST value (*Ts*) error is calculated using the uncertainty of each stress ratio. **Bold** numbers indicate ST best values of $Ts > 0.7$. The number and letter codes in the stress field correspond to the subareas identified in Fig. 5

as in Eq. (1). The ST plug-ins for Coulomb (Neves et al. 2009) were used to calculate ST. Here, the principal stress directions for the stress tensor, stress ratio $\phi (= (\sigma_2 - \sigma_3)/(\sigma_1 - \sigma_3))$, fault shape (strike and dip), and coefficient of friction on the fault were required to calculate the ST value (*Ts*). For the principal stress direction and stress ratio ϕ, the results from the estimated stress fields were used. For the fault shape, the nodal planes of the focal mechanisms and models estimated in NIED and in previous research were used (Aida 1984, 1989; Satake 1985, 1986; Kosuga et al. 1986; Sato 1993; Hirasawa 1965; Fukao and Furumoto 1975; Tanioka et al. 1995). The coefficient of friction was assumed to be 0.6 (Byerlee 1978). A method for evaluating ST error has not yet been established in previous studies. Therefore, this study thus attempted to evaluate ST error by first using the uncertainty of each stress ratio. We varied the stress ratio within the error range by 0.1, and calculated the ST value for each stress ratio.

Then, the range of ST value errors was defined as from the minimum to the maximum ST. The best ST value is that which uses the best stress ratio. Finally, in some cases, the changes in ST were confirmed using the changes in dip and strike (see Additional file 1: Table S1).

The study area was divided into two regions: (1) the EMJS area (lat. $37 - 42°$N, and lon. $137 - 141°$E; Fig. 1); (2) the Tohoku District inland area (lat. $36.5 - 41.5°$N and lon. $139 - 142°$E; Fig. 1). For each region, we focus on the large-to-moderate earthquakes: (1) the EMJS area: the 1833 Shonai-Oki earthquake M_{jma} 7.7, 1939 Oga earthquake M_{jma} 6.8, 1940 Shakotan-Oki earthquake M_{jma} 7.5, 1964 Niigata earthquake M_{jma} 7.5, 1983 Nihonkai-Chubu earthquake M_{jma} 7.7, 1993 Hokkaido Nansei-Oki earthquake M_{jma} 7.8, and 2019 Yamagata-Oki earthquake M_{jma} 6.7; (2) the Tohoku District inland area: the 1998 Shizukuishi earthquake M_{jma} 6.1, 2003 northern Miyagi earthquake M_{jma} 6.4, 2008 Iwate-Miyagi Nairiku earthquake M_{jma} 7.2, and 2016 Oshika Peninsula earthquake M_{jma} 5.2. The following workflow was applied to the earthquake in each region: (1) check the spatial and temporal distribution of the focal mechanisms using f-net data; (2) estimate the stress

field using regular gridding; (3) estimate the local stress fields around each large-to-moderate event; (4) calculate ST for each event.

Ranges for the local stress fields were determined based on the distribution and number of focal mechanisms. In addition, the stress fields were estimated using several range patterns to assess whether they would result in notable changes.

Results

EMJS area

Focal mechanism distributions

To identify the stress fields, events occurring between January 1, 1997 and June 17, 2019 were considered. The target area in the EMJS was lat. 37 − 42°N, and lon. 137 − 141°E. Only events at depths of 0–30 km were used. Focal mechanism distribution analysis showed that the reverse fault type was dominant in the study area (Fig. 2). The strike-slip fault type increased in the north when compared to that at lat. 39°N. Most of the focal mechanism P-axes tended to be NW–SE at latitudes below 40°N. Above 40°N, the P-axes tended to be in the E–W direction at depths of 0–10 km. This boundary was located at lat. 39°N for depths of 10–20 km and became ambiguous at depths of 20–30 km. The P-axis directions tended to be NW–SE in the Japan Sea and E–W in inland areas.

Stress field using regular gridding

The spatial variation in the stress field was first estimated using regular gridding. The target area was divided into small sub-areas (2° × 2°) to estimate the stress field (Figs. 3 and 4). The serial number in Fig. 4 (for example, E-1) shows the sub-area in Fig. 3. Consequently, in most of the subareas, the reverse fault type was dominant, except in the southeastern subarea (Fig. 3, Subarea E-10).

The maximum horizontal direction (S_{Hmax}) rotated clockwise from E–W to NW–SE from the northern to southern areas. Additionally, S_{Hmax} was rotated counterclockwise from NW–SE to E–W from the Japan Sea area to the coastal area. The uncertainties of S_{Hmax} in the inland areas were approximately 20.26–101.47°, which is larger than those in the Japan Sea area (approximately 9.74–28.46°).

ST method for large-to-moderate earthquakes using the local stress field

The likelihood of a fault slip was evaluated using the ST method. The ST value for seven large-to-moderate earthquakes was calculated and compared with actual fault activity. The target events were the 1833 Shonai-Oki earthquake M_{jma} 7.7, 1939 Oga earthquake M_{jma} 6.8, 1940 Shakotan-Oki earthquake M_{jma} 7.5, 1964 Niigata earthquake M_{jma} 7.5, 1983 Nihonkai-Chubu earthquake M_{jma} 7.7, 1993 Hokkaido Nansei-Oki earthquake M_{jma} 7.8, and 2019 Yamagata-Oki earthquake M_{jma} 6.7 (Fig. 1A). For

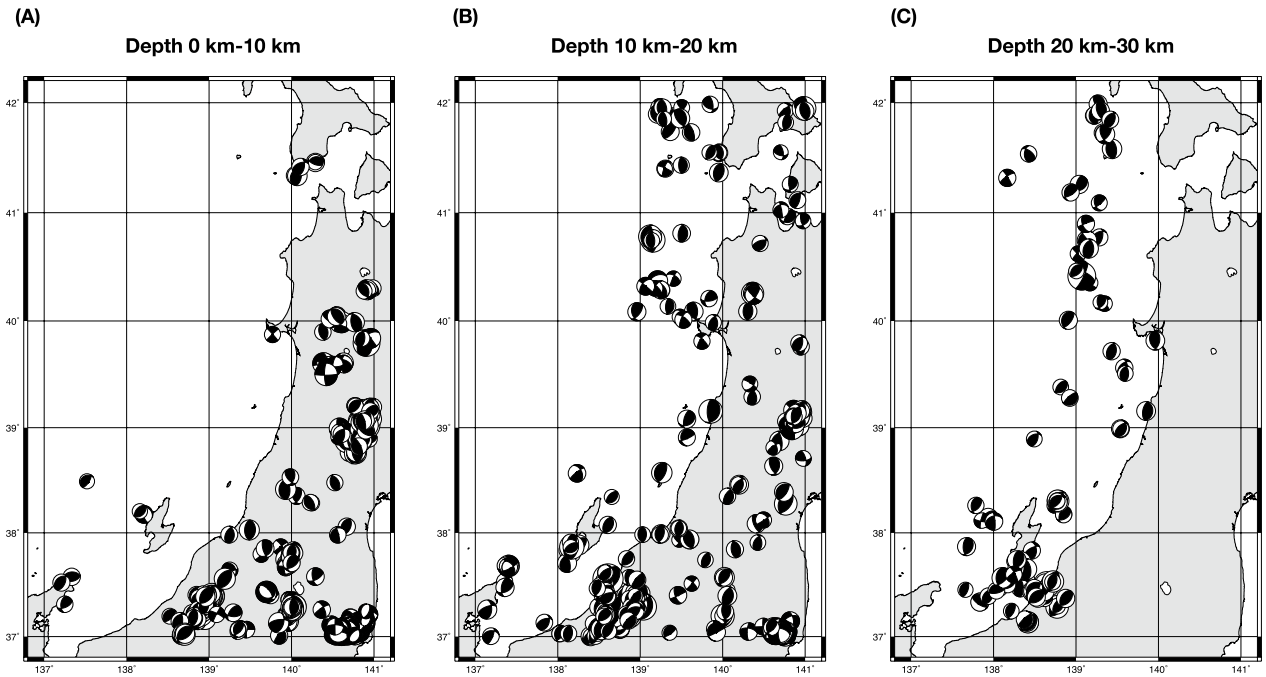

Fig. 2 Distribution of F-net focal mechanism solution in the eastern margin of the Japan Sea (EMJS). Each focal mechanism is plotted using the lower hemisphere projection. **A**, **B**, and **C** Events' distribution that occurred in depth 0–10 km, 10–20 km, and 20–30 km, respectively

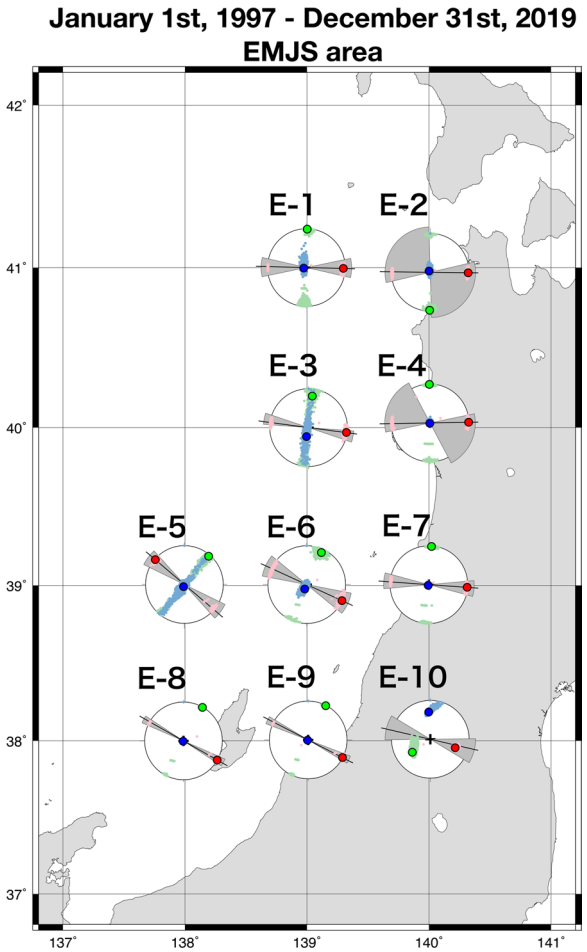

Fig. 3 Distribution of estimated stress field in the eastern margin of the Japan Sea (EMJS). Each result of stress field is plotted, 2° × 2°, at the center of each sub-area. The results are shown using lower hemisphere projections. Red, green, and blue circles denote the optimal solution for the σ_1, σ_2, and σ_3, respectively. Small pastel red, green, and blue without outlines denote the 95% confidence ranges for the σ_1, σ_2, and σ_3, respectively. The black line and gray fan denote the optimal solution and 95% confidence ranges for the S_{Hmax} orientation, respectively

six of the events (Oga, Shakotan-Oki, Niigata, Nihonkai-Chubu, Hokkaido Nansei-Oki, and Yamagata-Oki), the mainshock focal mechanisms were estimated from previous studies (F-net; Satake 1985, 1986; Sato 1993; Fukao and Furumoto 1975; Hirasawa 1965; Tanioka et al. 1995). The nodal plane for the focal mechanisms was then used to calculate ST. The ST values for the 1833 Shonai-Oki earthquake M_{jma} 7.7, 1983 Nihonkai-Chubu earthquake M_{jma}7.7, and 1993 Hokkaido-Nansei-Oki earthquake M_{jma} 7.8 were also estimated using fault models in previous studies (Aida 1984, 1989; Satake 1985; Kosuga et al. 1986; Tanioka et al. 1995).

Local stress field The stress field was estimated using only the focal mechanisms around each event to calculate the ST values for events that occurred between January 1, 1997, and December 31, 2019 (Fig. 5, the serial number shows regional area for each event). Each stress field showed a reverse fault type, and the S_{Hmax} trends were consistent with the results of regular gridding in the EMJS area (see above section and Figs. 3 and 4). Subsequently, ST was calculated for each nodal plane (Fig. 6). The uncertainty in the stress fields was estimated by changing the input stress ratio within each stress ratio uncertainty (Table 1).

ST value using nodal planes For the ST values of the nodal planes, all eastward-dipping planes with a lower dip angle showed larger ST values than the westward-dipping planes with a higher dip angle, except for the 1993 Hokkaido-Nansei-Oki earthquake MTRF (Moment Tensor Rate Functions) solution. The eastward-dipping planes had lower dip angles than those of the earthquakes, except for the 1993 Hokkaido-Nansei-Oki earthquake, and the ST values were $Ts > 0.7$. These planes were favorable for slipping into the stress field. For the 2019 Yamagata-Oki earthquake and the 1940 Shakotan-Oki earthquake, both planes were found to have large ST values ($Ts > 0.7$).

ST value using the fault model Two types of fault models were proposed by Aida (1989) for the 1833 Shonai-Oki earthquake. Model A is composed of two eastward-dipping planes: A-north and A-south, while Model B is composed of a westward-dipping plane. Based on Model A, the stress fields were estimated for three areas, as follows: "All" (entire focal area, denoted as "5-All" in Fig. 5), "Middle 1" (focal mechanisms around the fault model without events occurring inland, denoted as "5-Middle 1" in Fig. 5), and "Middle 2" (focal mechanisms around the model with events occurring inland, denoted as "5-Middle 2" in Fig. 5). For the stress field All, each model exhibited the ST value of approximately 0.6 (see Shonai-Oki earthquake in Table 2). For stress fields Middle 1 and Middle 2 (see Shonai-Oki earthquake in Table 2), the eastward-dipping plane (Model A) showed larger ST values ($Ts \sim 0.6 - 0.75$) than westward-dipping plane (Model B) ($Ts \sim 0.5$), and when using Middle 1, fault plane A-South had a large ST value ($Ts > 0.7$). The results indicate that Model A is more favorable for slipping than Model B.

Fault models for the 1983 Nihonkai-Chubu earthquake proposed in previous studies (Aida 1984; Satake 1985; Kosuga et al. 1986) were dipping in an eastward direction with a low dip angle (Fig. 6). Consequently, each model had a large ST value ($Ts > 0.7$) (Table 2) and the fault plane slipped as it was favorable for slipping into the stress field.

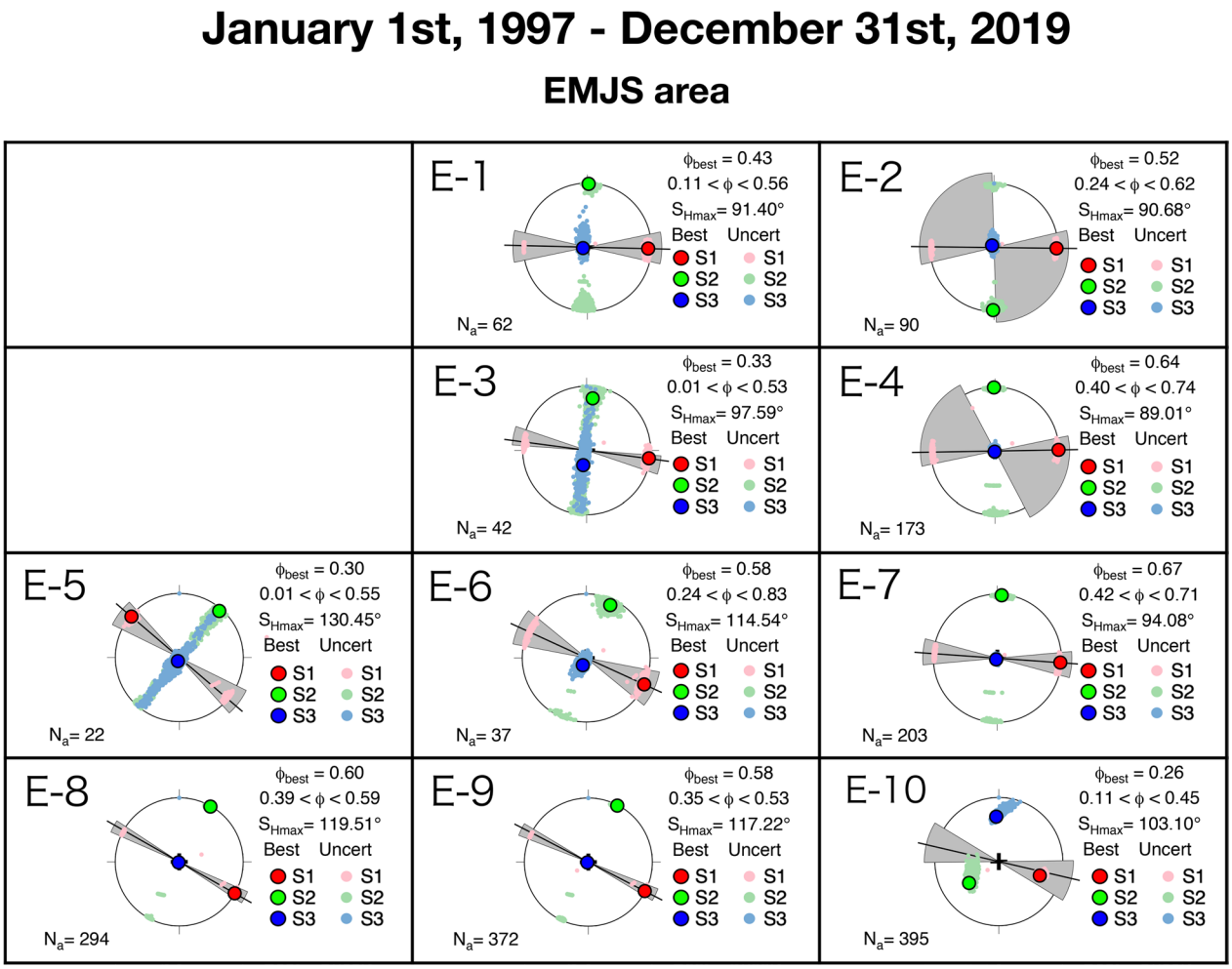

Fig. 4 Estimated stress field in the eastern margin of the Japan Sea (EMJS). ϕ_{best} is the optimal value of the stress ratio ($\phi(=\sigma_2-\sigma_3)/(\sigma_1-\sigma_3)$) with a 95% confidence range of ϕ. S_{Hmax} is the maximum horizontal compressional direction. N_a is the number of focal mechanisms used for each stress inversion in each area. The numbers in the upper left correspond to the subareas identified in Fig. 3

Tanioka et al. (1995) proposed a fault model for the 1993 Hokkaido Nansei-Oki earthquake, composed of one eastward-dipping plane with a low-dip-angle plane and two westward-dipping planes (Fig. 6). The eastward-dipping plane (A in Table 3) and westward-dipping planes with low dip angles (B and C in Table 3) showed ST values of $Ts > 0.7$. The westward-ipping planes with high dip angles (D and E in Table 3) had small ST values ($Ts < 0.6$). These results indicate that the fault planes with a low dip angle plane slipped and were considered favorable for slipping into the stress field.

Tohoku district inland area

Focal mechanism distributions

To calculate the stress fields, the events that occurred between January 1, 1997 and December 31, 2019 were considered. The target area for this study was the Tohoku District inland area at lat. 36.5 − 41.5°N and lon. 139 − 142°E. Only events at depths of 0–30 km were used. To consider the influence of the 2011 Tohoku-Oki earthquake, the data were divided into two periods: before the earthquake (January 1, 1997–March 10, 2011) and after the earthquake (March 11, 2011–December 31, 2019).

Assessments of the focal mechanism distributions showed that only a few events occurred at depths of 20–30 km. Prior to the Tohoku-Oki earthquake, the reverse fault type was dominant south of lat. 40°N (Fig. 7); the direction of the P-axis was E–W to NW–SE. After the Tohoku-Oki earthquake, multiple events occurred north of lat. 40°N; the direction of the P-axis was NE–SW, and the reverse fault type was dominant in this area. Additionally, the number of strike-slip types and normal fault types increased after the Tohoku-Oki

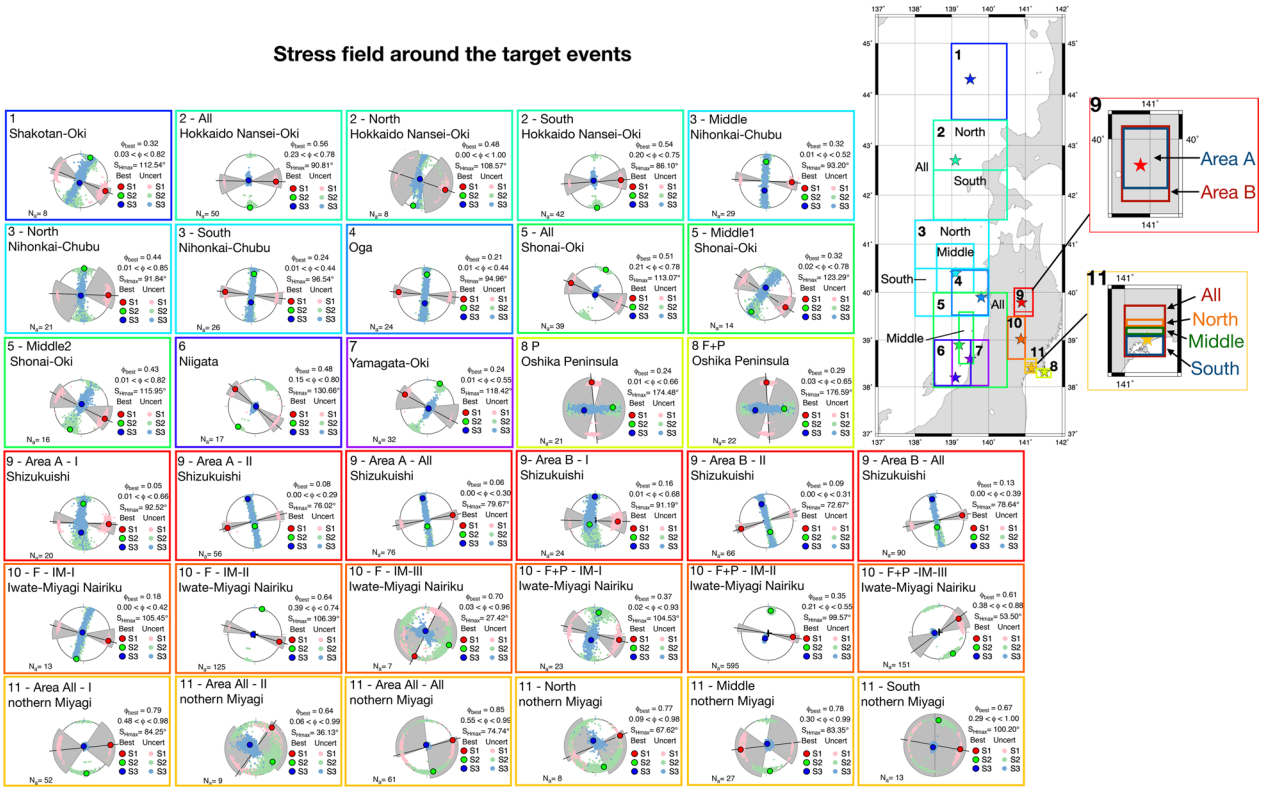

Fig. 5 Stress fields around each target event used for slip tendency analysis. Focal mechanism solutions were used in the area shown with the same-colored rectangle and the different numbers in the top left corner of each square indicate the earthquake event. The results are shown using lower hemisphere projections. Red, green, and blue circles denote the optimal solution for the σ_1, σ_2, and σ_3, respectively. Small pastel red, green, and blue without outlines denote the 95% confidence ranges for the σ_1, σ_2, and σ_3, respectively. The black line and gray fan denote the best and 95% confidence ranges for the S_{Hmax} orientation, respectively. ϕ_{best} is the best value for the stress ratio ($\phi(=\sigma_2-\sigma_3)/(\sigma_1-\sigma_3)$) and the 95% confidence range for ϕ. N_a is the number of focal mechanisms used for each stress inversion in each area

earthquake when compared to the data prior to the Tohoku-Oki earthquake.

Stress field using regular gridding

The spatial variations in the stress field were estimated using regular gridding, and the target area was divided into small regions ($1^\circ \times 1^\circ$). As there was a sufficient number of focal mechanisms, the region was divided into a finer grid than that used for the EMJS region. Consequently, the analysis showed that prior to the Tohoku-Oki earthquake, the stress field was dominant for the reverse fault type in this area. The S_{Hmax} direction was approximately E–W to WNW–ESE (Figs. 8 and 9). After the Tohoku-Oki earthquake, the S_{Hmax} directions were ENE–WSW to NE–SW in the northern area and NW–SE in the southern area.

The stress ratio prior to the Tohoku-Oki earthquake was 0.6–0.7; however, after the Tohoku-Oki earthquake, it changed from 0.2 to 0.5. On the east coast of the Miyagi and Fukushima prefectures, the uncertainty of the stress ratio increased after the Tohoku-Oki earthquake, and this may be attributed to various focal mechanisms.

ST method for large-to-moderate earthquakes using the local stress field

The likelihood of a fault slip was evaluated using the ST method. The ST value for four large-to-moderate earthquakes was calculated and compared with actual fault activity.

The target events were the 1998 Shizukuishi earthquake M_{jma} 6.1, 2003 northern Miyagi earthquake M_{jma} 6.4, 2008 Iwate-Miyagi Nairiku earthquake M_{jma} 7.2, and 2016 Oshika Peninsula earthquake M_{jma} 5.2 (Fig. 1).

Focal mechanism data split by period The stress field was estimated using only the focal mechanisms that occurred between January 1, 1997 and December 31, 2019, around each event. Considering the number of mechanism solutions and the influence of the 2011

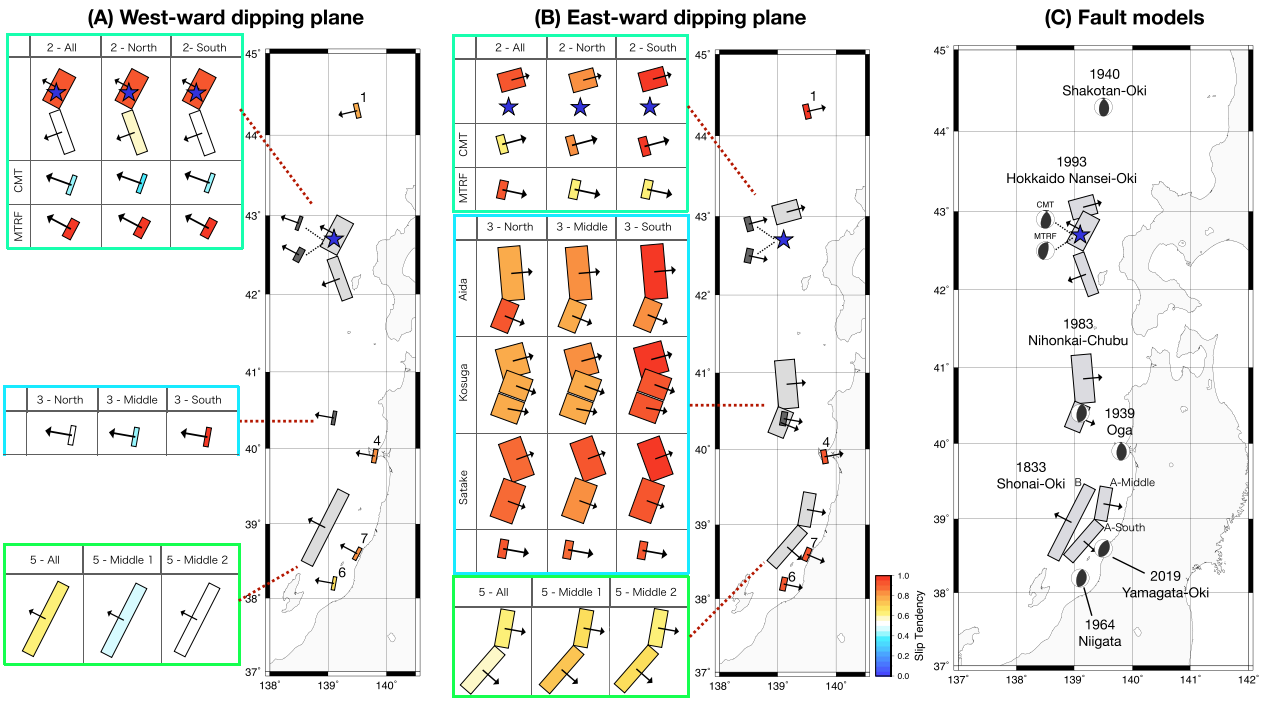

Fig. 6 Slip tendency (ST) values for the eastern margin of the Japan Sea (EMJS). **A** The ST values with westward-dipping plane. **B** The ST values with eastward-dipping plane. **C** The distribution of the target events. The left boxes in **A**, **B** The ST value of fault model. The color of the nodal plane shows the ST value. The arrows on the nodal plane denote the dipping directions. The number written at the top of each box indicates the stress field in Fig. 5 used to calculate ST value

Tohoku-Oki earthquake, the data were divided into three terms for the 1998 Shizukuishi and 2003 northern Miyagi earthquakes: "term-I" (January 1, 1997 to March 10, 2011); "term-II" (March 11, 2011 to December 31, 2019); and "term-All" (January 1, 1997 to December 31, 2019).

The 2008 Iwate-Miyagi Nairiku earthquake had a sufficient number of focal mechanisms to enable estimations of the stress field. The magnitude of the 2008 Iwate-Miyagi Nairiku earthquake was estimated as M_{jma} 7.2. Stress changes were confirmed to occur after the large earthquake and thus may have also occurred after the 2008 Iwate-Miyagi Nairiku earthquake. To investigate whether stress changes occurred and affected the ST values, focal mechanism data were divided into three terms: "IM (Iwate-Miyagi)-I" (January 1, 1997 to June 13, 2008); "IM-II" (June 14, 2008 to March 10, 2011); and "IM-III" (March 11, 2011 to December 31, 2019).

The 2016 Oshika Peninsula earthquake had only a few focal mechanisms, and consequently, only the events that occurred after the 2011 Tohoku-Oki earthquake were used. Additionally, only a few focal mechanisms were available for the F-net catalog, and consequently, the focal mechanism data estimated from the P-wave initial motions from Okada et al. (2015; 2022) were added.

As an overall trend, each event showed a reverse or strike-slip fault type (8, 9, 10, and 11 in Fig. 5). The S_{Hmax} trends were consistent with the results for regular gridding in the Tohoku District inland area (see above section) (Fig. 8).

Local stress field and the ST value 1998 Shizukuishi earthquake

The results for the 1998 Shizukuishi earthquake were assessed first. Based on the focal mechanism distribution, it was possible to investigate several patterns in the local areas, and two types in the region (Area A and Area B in Fig. 5) were assessed for spatial changes. From the results of the 1998 Shizukuishi earthquake, the estimated stress field in Area A showed a reverse fault type solution in term-I (see 9—Area A-I in Fig. 5), and Area B showed a strike-slip fault type (see 9—Area B-I in Fig. 5). However, the uncertainties for both σ_2 and σ_3 overlapped and the S_{Hmax} directions indicated E–W. Therefore, the stress fields for Areas A and B had approximately the same results in term-I. Term-II and term All showed strike-slip fault type solutions, with the S_{Hmax} direction being ENE–WSW, while the uncertainties for σ_2 and σ_3 overlapped (see 9-Area A-II and 9-Area A-All in Fig. 5). More data were used for term-II than term All, and consequently, the stress field for term All was considered to be similar to that of term-II.

Table 2 Slip tendency (ST) for 1833 Shonai-Oki and 2008 Nihonkai-Chubu earthquakes calculated using fault models

Events	Fault model		Dip direction	Stress field	*Ts* best	*Ts* error
Shonai-Oki earthquake	Aida (1989)	A-North	East	5—All	0.604	$0.598 < Ts < 0.671$
		A-South	East		0.578	$0.559 < Ts < 0.623$
		B	West		0.603	$0.603 < Ts < 0.603$
		A-North	East	5—Middle 1	0.676	$0.571 < Ts < 0.834$
		A-South	East		**0.742**	$0.740 < Ts < 0.744$
		B	West		0.461	$0.461 < Ts < 0.461$
		A-North	East	5 -Middle 2	0.619	$0.588 < Ts < 0.702$
		A-South	East		0.676	$0.669 < Ts < 0.693$
		B	West		0.536	$0.534 < Ts < 0.542$
Nihonkai-Chubu earthquake	Aida (1984)	North	East	3—North	**0.798**	$0.798 < Ts < 0.798$
		South	East		**0.949**	$0.948 < Ts < 0.997$
		North	East	3—Middle	**0.843**	$0.843 < Ts < 0.905$
		South	East		**0.783**	$0.724 < Ts < 0.986$
		North	East	3—South	**0.956**	$0.948 < Ts < 0.987$
		South	East		**0.827**	$0.773 < Ts < 0.925$
	Kosuga et al. (1986)	North	East	3—North	**0.770**	$0.769 < Ts < 0.780$
		South	East		**0.766**	$0.752 < Ts < 0.837$
		North	East	3—Middle	**0.847**	$0.846 < Ts < 0.885$
		South	East		**0.758**	$0.757 < Ts < 0.879$
		North	East	3—South	**0.960**	$0.957 < Ts < 0.977$
		South	East		**0.900**	$0.873 < Ts < 0.983$
	Satake (1985)	North	East	3—North	**0.881**	$0.878 < Ts < 0.902$
		South	East		**0.883**	$0.879 < Ts < 0.933$
		North	East	3—Middle	**0.925**	$0.924 < Ts < 0.957$
		South	East		**0.800**	$0.782 < Ts < 0.961$
		North	East	3—South	**0.991**	$0.989 < Ts < 0.998$
		South	East		**0.905**	$0.866 < Ts < 0.994$

ST value (*Ts*) error is calculated using the uncertainty of each stress ratio. **Bold** numbers indicate ST best values of $Ts > 0.7$. The number and letter codes in the stress field correspond to the subareas identified in Fig. 5

Table 3 Slip tendency (ST) for 1993 Hokkaido Nansei-Oki earthquake calculated using fault models

Events	Fault model		Dip direction	Stress field	*Ts* best	*Ts* error
Hokkaido Nansei-Oki earthquake	Tanioka et al. (1995)	A	East	2—All	**0.947**	$0.943 < Ts < 0.960$
		B, C	East		**0.943**	$0.943 < Ts < 0.961$
		D, E	West		0.513	$0.497 < Ts < 0.562$
		A	East	2—North	**0.815**	$0.787 < Ts < 0.996$
		B, C	East		**0.935**	$0.933 < Ts < 0.953$
		D, E	West		0.586	$0.525 < Ts < 0.821$
		A	East	2—South	**0.955**	$0.953 < Ts < 0.964$
		B, C	East		**0.929**	$0.929 < Ts < 0.957$
		D, E	West		0.507	$0.497 < Ts < 0.537$

ST value (*Ts*) error is calculated using the uncertainty of each stress ratio. **Bold** numbers indicate ST best values of $Ts > 0.7$. The number and letter codes in the stress field correspond to the subareas identified in Fig. 5

The results of the ST method showed that both nodal planes had large ST values ($Ts > 0.7$) (9 in Fig. 10, values are shown in Table 4). The differences in ST values were small (< 0.1) for most terms, but both nodal planes were favorable for slipping into the stress field.

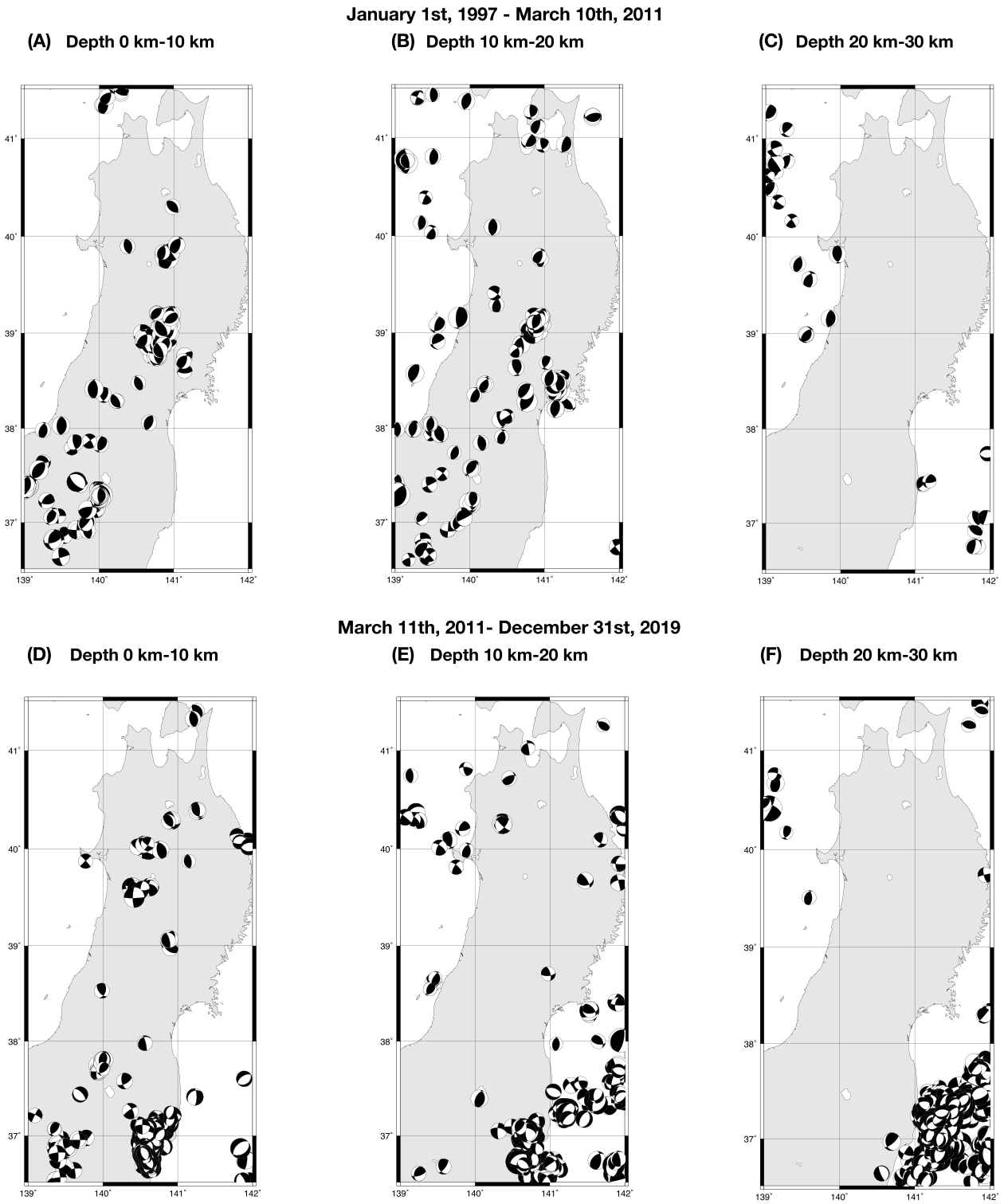

Fig. 7 Distribution of F-net focal mechanism solution in the Tohoku District inland area. Each focal mechanism is plotted using the lower hemisphere projection. **A**, **B**, and **C** The events that occurred from January 1, 1997 to March 10, 2011 (before the Tohoku-Oki earthquake). **D**, **E**, and **F** The events that occurred from March 11, 2011 to December 31, 2019 (after the Tohoku-Oki earthquake). **A** and **D**, **B** and **E**, and **C** and **F** Events' distribution that occurred in depth 0–10 km, 10–20 km, and 20–30 km, respectively

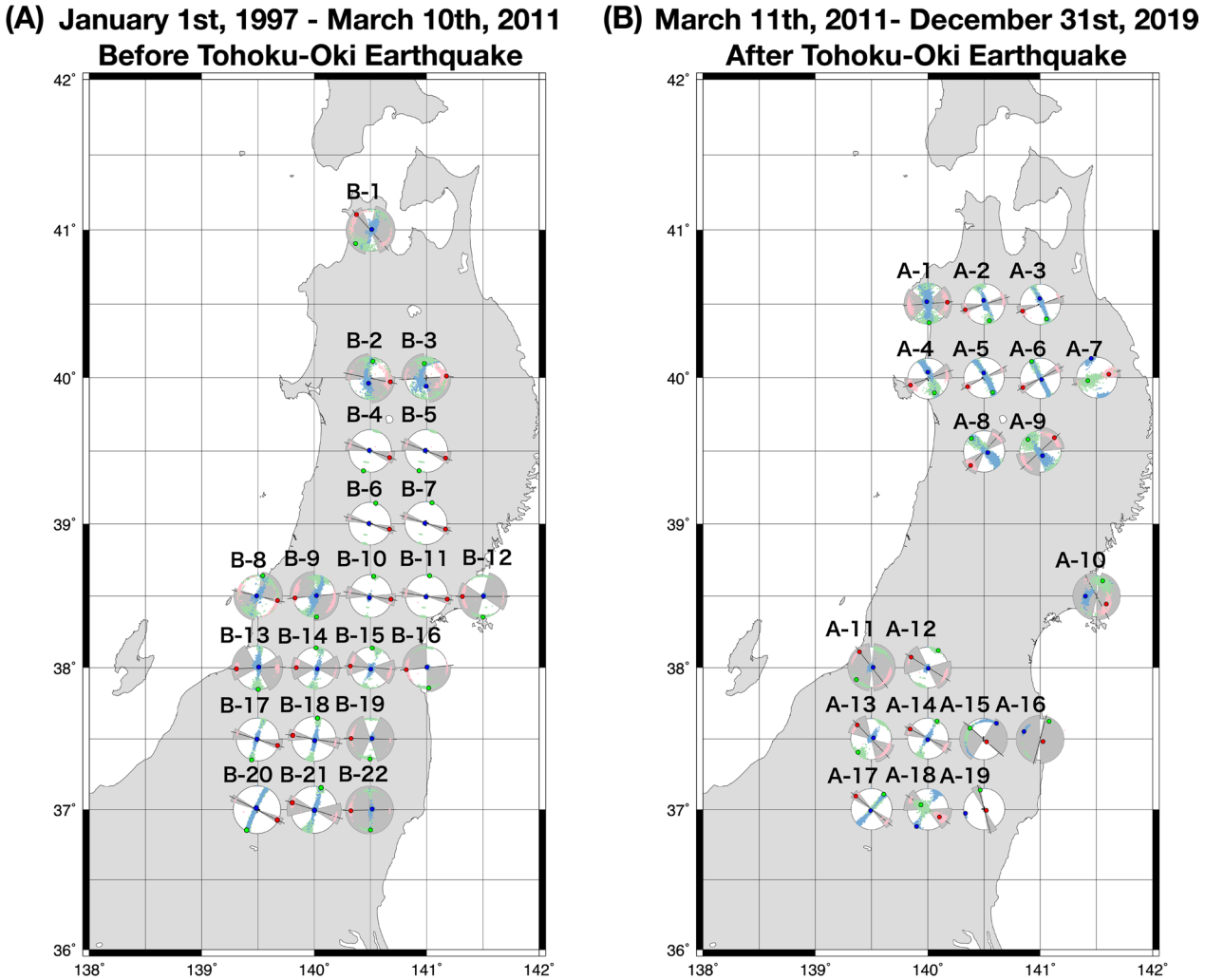

Fig. 8 Distribution of the estimated stress field in the Tohoku District inland area. Each result is plotted, 1° × 1°, at the center of each sub-area. **A**, **B** The events that occurred from January 1, 1997 to March 10, 2011 (before the Tohoku-Oki earthquake) and from March 11, 2011 to December 31, 2019 (after the Tohoku-Oki earthquake), respectively. The results are shown using lower hemisphere projections. Red, green, and blue circles denote the optimal solution for σ_1, σ_2, and σ_3, respectively. Small pastel red, green, and blue without outlines denote the 95% confidence ranges for σ_1, σ_2, and σ_3, respectively. The black line and gray fan denote the best and the 95% confidence ranges for the S_{Hmax} orientation, respectively

2003 northern Miyagi earthquake

From the results of the 2003 northern Miyagi earthquake, the eastward-dipping plane showed a large ST value ($Ts > 0.7$) for most terms (11 in Fig. 10, values are shown in Table 5). After the Tohoku-Oki earthquake (term-II), however, the ST value was reduced (11–II in Fig. 10). However, the eastward-dipping plane with a low dip angle had a larger ST value than the westward-dipping plane with a high dip angle in each term.

The largest foreshock (M_{jma} 5.6) and largest aftershock (M_{jma} 5.5) of the 2003 northern Miyagi earthquake were also assessed (Fig. 10). In the study area, the largest aftershocks and foreshocks occurred in the northern and middle regions, respectively, while the main shocks occurred in the southern region (see Fig. 10). Based on these locations, the study area was divided into three regions (North, Middle, and South) for stress field estimations (11-North, 11-Middle, and 11-South in Fig. 5). Each area represents a reverse fault type for the stress field, and accordingly, the ST values for each event were calculated. The mainshock and largest foreshock had larger ST values in the eastward-dipping plane with a low dip angle. However, the largest aftershock in the westward-dipping plane with a high dip angle plane showed a large ST value ($Ts > 0.7$), which was larger than that of the eastward-dipping plane (Fig. 10 and Table 5).

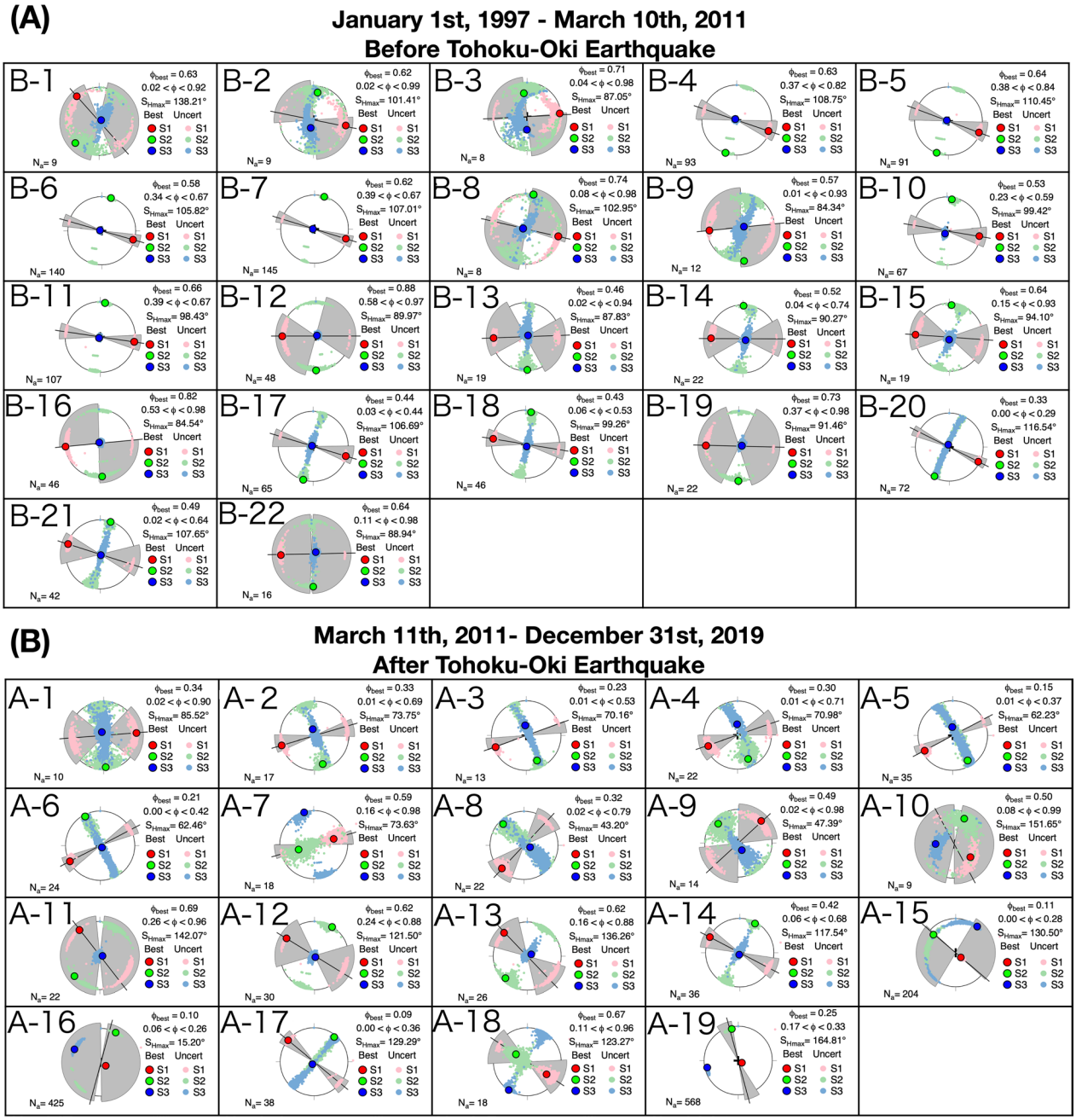

Fig. 9 Estimated stress field in the Tohoku District inland area. **A**, **B** The estimated stress field using data from January 1, 1997 to March 10, 2011 (before the Tohoku-Oki earthquake) and from March 11, 2011 to December 31, 2019 (after the Tohoku-Oki earthquake), respectively. The number and letter codes in the upper left corners of each square correspond to the subareas identified in Fig. 8. Red, green, and blue circles denote the optimal solution for σ_1, σ_2, and σ_3, respectively. Small pastel red, green, and blue without outlines denote the 95% confidence ranges for σ_1, σ_2, and σ_3, respectively. The black line and gray fan denote the best and the 95% confidence ranges for the S_{Hmax} orientation, respectively. ϕ_{best} is the optimal value for the stress ratio ($\phi(=\sigma_2-\sigma_3)/(\sigma_1-\sigma_3)$) at a 95% confidence range of ϕ. N_a= is the number of focal mechanisms used for each stress inversion in each area

2008 Iwate-Miyagi Nairiku earthquake

For the 2008 Iwate-Miyagi Nairiku earthquake, each term represented a reverse fault type for the stress field. As the two databases each had a sufficient number of solutions, the difference in the stress fields was also evaluated first using only F-net data (10-F in Fig. 5) and again after adding Okada data (10-F + P in Fig. 5). There were no significant changes between stress fields determined using the

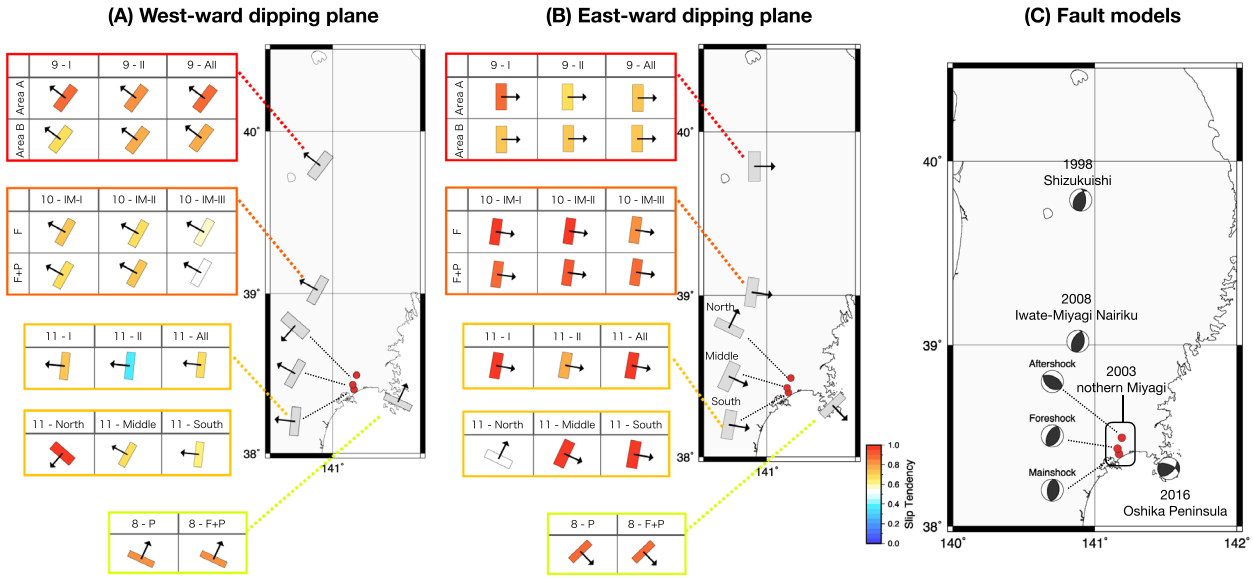

Fig. 10 Slip tendency (ST) values for the Tohoku District inland area. **A** The ST values with westward-dipping plane. **B** The ST values with eastward-dipping plane. **C** The distribution of the target events. The left boxes in panels **A** and **B** show the ST value of the fault model. The color of the nodal plane shows the ST value. The arrows on the nodal plane denote the dipping directions. The number written at the top of each box indicates the stress field in Fig. 5 used to calculate ST value

10-F and 10-F + P data. However, more focal mechanisms resulted when using the 10-F + P than the 10-F data. The 10-F + P solution thus showed smaller uncertainty than the 10-F solution. Regarding the temporal change, the S_{Hmax} directions were WNW–ESE in 10-IM-I and 10-IM-II and NE–SW in 10-IM-III (Fig. 5). The uncertainty of σ_2 and σ_3 directions overlapped in 10-IM-I, and the stress field had a strike-slip component (Fig. 5).

From the ST method results, the nodal plane with an eastward-dipping plane and with a low dip angle showed a large ST value ($Ts > 0.7$) for all terms (Fig. 10 and Table 4). The eastward-dipping plane was favorable for slipping into the stress field.

2016 Oshika Peninsula earthquake

The stress field was transpressive during the 2016 Oshika Peninsula earthquake (8 P and 8 F + P in Fig. 5), and the direction of the S_{Hmax} was N–S. The results of the ST method showed that both nodal planes had large ST values ($Ts > 0.7$; Fig. 10 and Table 5); however, the differences in ST values were small ($Ts < 0.1$). Both nodal planes were favorable for slipping into the stress field, and other factors might have influenced the selection of the slip plane.

Discussion

Effect of fault plane selection on stress field estimation

The stress fields were estimated for the 2003 northern Miyagi earthquake M_{jma} 6.4 and the 2016 Oshika Peninsula earthquake M_{jma} 5.2, but they contained wide uncertainties and were not stable. Consequently, the stress fields for these two earthquakes were re-estimated using the slip instability method (Vavryčuk et al. 2013; Vavryčuk 2014) and the results were compared.

The focal mechanism has two nodal planes: the fault plane and the auxiliary plane. To apply an assumption of the Wallace–Bott hypothesis, the nodal plane for the fault must be determined; however, this is only possible by distinguishing the fault plane using other information (e.g., coseismic surface faults and aftershock distributions). With Michael's method, the fault plane is randomly selected from the two nodal planes of each focal mechanism. The incorrect selection of auxiliary surfaces can lead to biased results and unstable solutions with large uncertainties. Vavryčuk et al. (2013) defined fault instability (I) based on Lund and Slunga (1999) as follows:

$$I = \frac{\tau - \mu(\sigma - \sigma_1)}{\tau_c - \mu(\sigma_c - \sigma_1)}, \tag{2}$$

where μ is the coefficient of the friction; τ_c and σ_c are the shear and normal stresses along the fault in the optimal orientation, respectively; τ and σ are the shear and normal stresses along the analyzed fault plane, respectively; and σ_1 is the maximum principal stress. Consequently, Eq. (2) does not depend on absolute stress values, and I can only be evaluated from μ, the shape ratio $R(= 1 - \phi = (\sigma_1 - \sigma_2)/(\sigma_1 - \sigma_3))$, and the directional

Table 4 Slip tendency (ST) for 1998 Shizukuishi and 2008 Iwate-Miyagi Nairiku earthquakes calculated using focal mechanism

Events	Fault model	Dip direction	Stress field	*Ts* best	*Ts* error
Shizukuishi earthquake	F-net	East	9-Area A–I	**0.884**	$0.792 < Ts < 0.895$
		West	1997–2011	**0.885**	$0.883 < Ts < 0.885$
		East	9–Area A–II	0.697	$0.576 < Ts < 0.752$
		West	2011–2019	**0.839**	$0.589 < Ts < 0.980$
		East	9–Area A–All	**0.744**	$0.585 < Ts < 0.791$
		West	1997–2019	**0.891**	$0.572 < Ts < 0.998$
		East	9–Area B–I	**0.733**	$0.246 < Ts < 0.968$
		West	1997–2011	0.650	$0.375 < Ts < 0.770$
		East	9–Area B–II	**0.746**	$0.692 < Ts < 0.772$
		West	2011–2019	**0.774**	$0.463 < Ts < 0.956$
		East	9–Area B–All	**0.724**	$0.567 < Ts < 0.825$
		West	1997–2019	**0.786**	$0.491 < Ts < 0.999$
Iwate-Miyagi Nairiku earthquake	F-net	East	10–F–IM–I	**0.955**	$0.949 < Ts < 0.963$
		West	1997–2008 (F-net)	**0.704**	$0.685 < Ts < 0.724$
		East	10–F–IM–II	**0.967**	$0.967 < Ts < 0.968$
		West	2008–2011 (F-net)	0.679	$0.678 < Ts < 0.686$
		East	10–F–IM–III	**0.813**	$0.732 < Ts < 0.910$
		West	2011–2019 (F-net)	0.578	$0.356 < Ts < 0.662$
		East	10–F + P–IM–I	**0.876**	$0.784 < Ts < 0.982$
		West	1997–2008 (F-net and P wave polarity)	0.660	$0.636 < Ts < 0.676$
		East	10–F + P–IM–II	**0.949**	$0.942 < Ts < 0.960$
		West	2008–2011 (F-net and P wave polarity)	**0.707**	$0.704 < Ts < 0.710$
		East	10–F + P–IM–III	**0.865**	$0.823 < Ts < 0.952$
		West	2011–2019 (F-net and P wave polarity)	0.540	$0.527 < Ts < 0.622$

ST value (*Ts*) error is calculated using the uncertainty of each stress ratio. **Bold** numbers indicate ST best values of $Ts > 0.7$. The number and letter codes in the stress field correspond to the subareas identified in Fig. 5

cosines **n** which define the inclination of the fault plane from the principal stress axis. It can thus be normalized using $\sigma_1 = -1$, $\sigma_2 = 2R - 1$, and $\sigma_3 = 1$, as follows:

$$I = \frac{\tau + \mu(\sigma + 1)}{\mu + \sqrt{1 + \mu^2}}. \tag{3}$$

It then follows that

$$\sigma = -n_1^2 + (2R - 1)n_2^2 + n_3^2 \tag{4}$$

$$\tau = \sqrt{n_1^2 + (2R - 1)^2 n_2^2 + n_3^2 - \left(-n_1^2 + (2R - 1)n_2^2 + n_3^2\right)^2} \tag{5}$$

where I is expressed between 0 and 1. When $I = 1$, the fault plane is in its most unstable state, and this indicates that the nodal plane is the principal fault plane. The fault plane can thus be selected from the two nodal planes using I, and the stress field can be estimated using a narrower confidence range than that in Michael's method if this selection is adequate.

To assess the effect of the fault plane selection on the stress tensor inversion, Vavryčuk's method was applied to re-estimate the stress field of the 2003 northern Miyagi earthquake M_{jma} 6.4 and 2016 Oshika Peninsula earthquake M_{jma} 5.2.

2003 northern Miyagi earthquake M_{jma} 6.4

For all periods and ranges, the results did not differ significantly from those obtained using Michael's method (Figs. 5 and 11, and Table 6). The results re-estimated using Vavryčuk's method had smaller uncertainties in σ_1, σ_2, and σ_3 directions (Fig. 11) compared with the results estimated using Michael's method. The optimal values for the stress ratio (ϕ_{Best}) and optimal S_{Hmax} direction

Table 5 Slip tendency (ST) for 2003 Miyagi and 2016 Oshika Peninsula earthquakes calculated using focal mechanism

Events	Fault model	Dip direction	Stress field	*Ts* best	*Ts* error
Northern Miyagi earthquake mainshock	F-net	East	11–Area All–I	**0.960**	$0.959 < Ts < 0.962$
		West	1997–2011	**0.717**	$0.717 < Ts < 0.725$
		East	11–Area All–II	**0.790**	$0.732 < Ts < 0.888$
		West	2011–2019	0.380	$0.352 < Ts < 0.884$
		East	11–Area All–All	**0.975**	$0.971 < Ts < 0.980$
		West	1997–2019	0.672	$0.672 < Ts < 0.687$
		East	11–South	**0.981**	$0.980 < Ts < 0.986$
		West	1997–2011	0.639	$0.638 < Ts < 0.645$
Largest foreshock	F-net	East	11–Middle	**0.950**	$0.946 < Ts < 0.964$
		West	1997–2011	0.673	$0.673 < Ts < 0.771$
Largest aftershock	F-net	East	11–North	0.508	$0.506 < Ts < 0.869$
		West	1997–2011	**0.981**	$0.981 < Ts < 0.982$
Oshika peninsula earthquake	F-net	SE	8–F + P	**0.887**	$0.881 < Ts < 0.895$
		NE	(F-net and P wave polarity)	**0.824**	$0.824 < Ts < 0.824$
		SE	8–P	**0.877**	$0.863 < Ts < 0.893$
		NE	(P wave polarity)	**0.812**	$0.805 < Ts < 0.819$

ST value (*Ts*) error is calculated using the uncertainty of each stress ratio. **Bold** numbers indicate ST best values $Ts > 0.7$. The number and letter codes in the stress field correspond to the subareas identified in Fig. 5

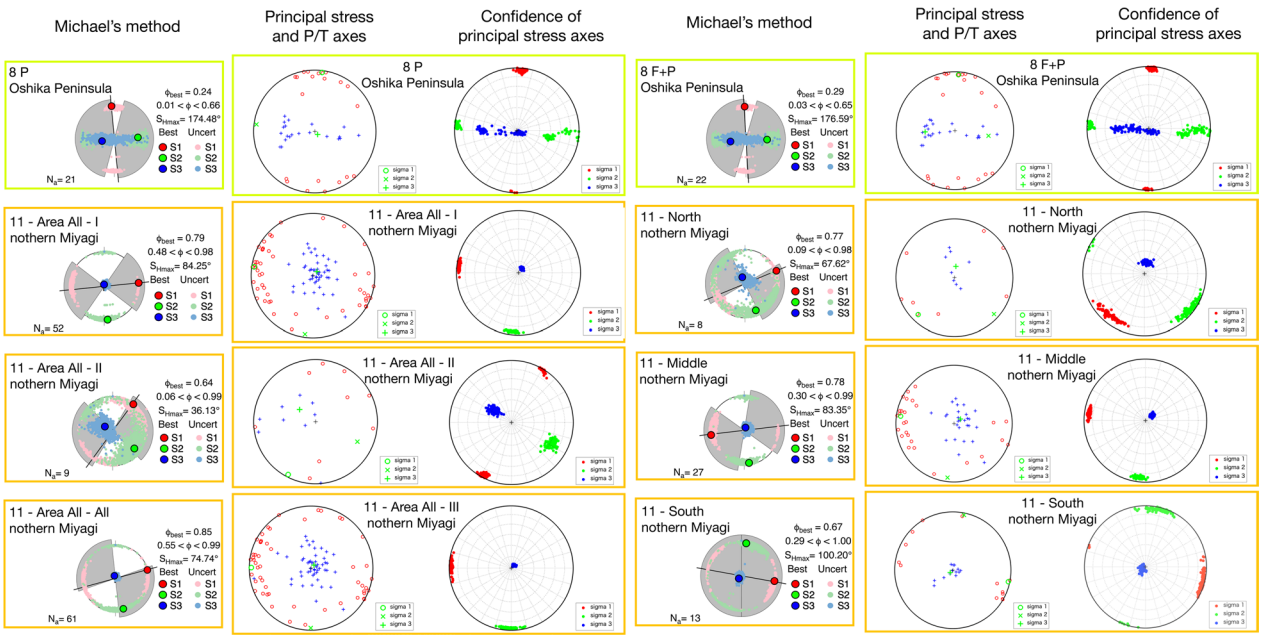

Fig. 11 Analysis of the estimated stress field using slip instability methods. The results are shown using lower hemisphere projections. In the left circle of the slip instability results, the blue plus mark and red circle denote the T and P axes, respectively. The green circle, cross, and plus mark denote the best direction for σ_1, σ_2, and σ_3, respectively. The red, green, and blue dots denote the uncertainty of σ_1, σ_2, and σ_3, respectively. The results using Michael's method and the name of each area (for example "8P Oshika Peninsula") are the same as those in Fig. 5

($S_{HmaxBest}$) were slightly changed, but were within the error range for the results estimated using Michael's method.

2016 Oshika peninsula earthquake M_{jma} 5.2

Using only the P-wave polarity data, the stress field was shown to have a transpressive type, which was closer to the reverse fault type (8 P in Fig. 11, values are shown

Table 6 Stress field parameters for the 2003 northern Miyagi earthquake

Area	Michael's method				Slip instability method			
	σ1 azimuth plunge	σ2 azimuth plunge	σ3 azimuth plunge	φ min best max	σ1 azimuth plunge	σ2 azimuth plunge	σ3 azimuth plunge	φ min best max
11–Area All–I	84	174	– 8	0.48	276	185	50	0.57
	0	4	86	0.79	6	6	82	0.64
				0.98				0.72
11–Area All–II	38	129	– 60	0.06	208	115	307	0.24
	3	21	69	0.64	5	26	64	0.45
				0.99				0.74
11–Area All–All	7	165	– 22	0.55	272	182	17	0.63
	1	7	83	0.85	1	5	84	0.72
				0.99				0.78
11–North	68	158	– 23	0.09	225	133	7	0.40
	0	17	73	0.77	13	9	74	0.47
				0.98				0.77
11–Middle	– 98	172	25	0.3	278	187	55	0.39
	4	6	83	0.78	8	8	79	0.55
				0.99				0.77
11–South	99	8	– 137	0.29	102	12	230	0.52
	5	7	81	0.67	3	4	85	0.67
				1.00				0.81

The number and letter codes in the Area column correspond to the subareas identified in Figs. 5 and 11

Table 7 Stress field parameters for the 2016 Oshika Peninsula earthquake

Area	Michael's method				Slip instability method			
	σ1 azimuth plunge	σ2 azimuth plunge	σ3 azimuth plunge	φ min best max	σ1 azimuth plunge	σ2 azimuth plunge	σ3 azimuth plunge	φ min best max
8–P	– 5	87	– 101	0.01	7	277	136	0.16
	3	31	59	0.24	3	4	85	0.29
				0.66				0.39
8–F + P	– 2	92	– 100	0.03	4	99	268	0.16
	6	38	52	0.29	6	42	48	0.32
				0.65				0.39

The number and letter codes in the Area column correspond to the subareas identified in Figs. 5 and 11

in Table 7). Including the F-net data, the stress field was transpressive (8 P + F in Fig. 11, values are shown in Table 7), and was similar to the results estimated using Michael's method (Fig. 11). The uncertainty of each principal-stress direction was smaller than that estimated using Michael's method, and the ϕ_{Best} and $S_{HmaxBest}$ did not change significantly. The re-estimated stress fields were almost the same as those estimated using Michael's method.

Effect on the ST value

ST values were calculated using the re-estimated stress fields (Fig. 12 and Table 8). Focusing on the ST values, the results of the 2016 Oshika Peninsula earthquake showed almost the same results as previously (see Results, section). The best principal stress axis in the results using only the P-wave polarity data (8 P in Fig. 11) showed a reverse fault type. However, uncertainty of the principal stress directions in the results determined using Michael's method and Vavryčuk's method were overlapping (8 P in Fig. 11), and consequently, no significant change was identified. The uncertainty of the ST value became smaller than that obtained from the stress tensor inversion results using Michael's method (Michael's stress field; Tables 5 and 8). This may be because the uncertainty of the stress ratio was smaller than that of the previous one (Tables 6 and 7). The best principal axis in the results using only the P-wave polarity data in the 2016

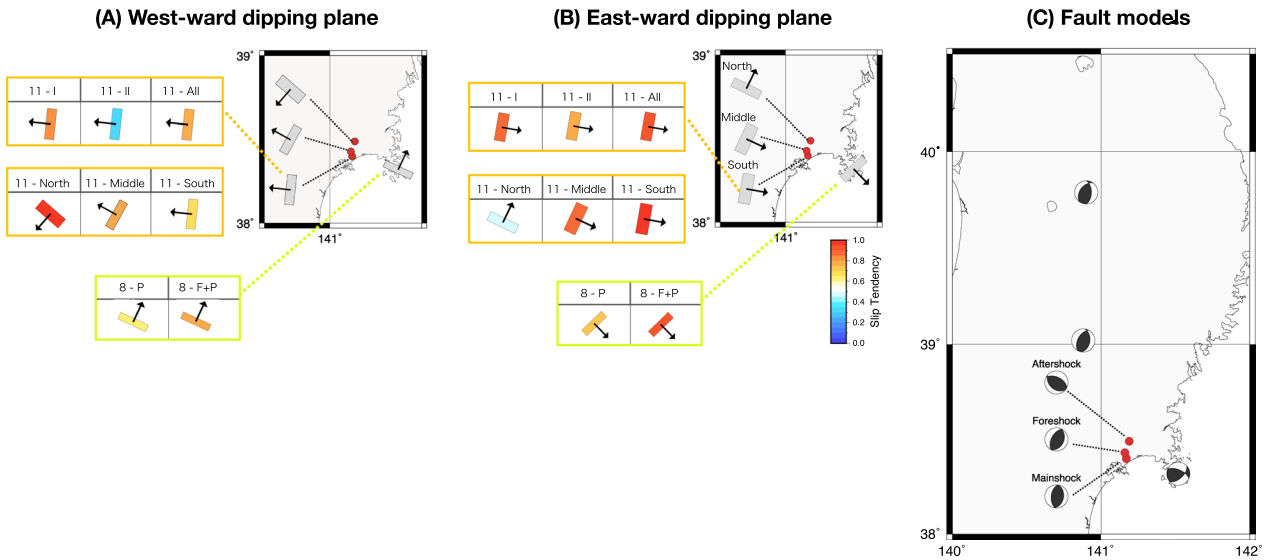

Fig. 12 Slip tendency (ST) values determined using the stress parameter estimated with the slip instability method. **A** The ST values with westward-dipping plane. **B** The ST values with eastward-dipping plane. **C** The distribution of the target events. The left boxes in **A** and **B** show the ST value of the fault model. The color of the nodal planes indicates the ST value. The arrows on the nodal plane denote the dipping directions. The number written at the top of each box indicates the stress field in Fig. 11 used to calculate ST value

Table 8 Slip tendency (ST) determined using stress field parameters estimated by the slip instability method

Events	Fault model	Dip direction	Stress field	*Ts* best	*Ts* error
Northern Miyagi earthquake mainshock	F-net	East	11–Area All–I	**0.876**	$0.876 < Ts < 0.876$
		West	1997–2011	**0.834**	$0.834 < Ts < 0.835$
		East	11–Area All–II	**0.759**	$0.745 < Ts < 0.806$
		West	2011–2019	0.316	$0.272 < Ts < 0.427$
		East	11–Area All–III	**0.939**	$0.939 < Ts < 0.939$
		West	1997–2019	**0.756**	$0.755 < Ts < 0.756$
		East	11–South	**0.977**	$0.977 < Ts < 0.977$
		West	1997–2011	0.677	$0.677 < Ts < 0.679$
Largest foreshock	F-net	East	11–Middle 1997–2011	**0.894**	$0.894 < Ts < 0.895$
		West		**0.777**	$0.767 < Ts < 0.799$
Largest aftershock	F-net	East	11–North 1997–2011	0.489	$0.457 < Ts < 0.500$
		West		**0.984**	$0.983 < Ts < 0.987$
Oshika peninsula earthquake	F-net	SE	8–F + P	**0.946**	$0.945 < Ts < 0.950$
		NE	(F-net and P-wave polarity)	**0.753**	$0.752 < Ts < 0.758$
		SE	8–P	**0.709**	$0.653 < Ts < 0.814$
		NE	(P-wave polarity)	0.639	$0.624 < Ts < 0.664$

ST value (*Ts*) error is calculated using the uncertainty of each stress ratio. **Bold** numbers indicate ST best values of $Ts > 0.7$. The number and letter codes in the stress field correspond to the subareas identified in Figs. 5 and 11

Oshika Peninsula earthquake showed an approximate reverse fault type (8 P in Fig. 11). Using the same dataset the results showed a transpressive type when using Michael's method (Fig. 11). These results were probably due to the differences in the selection of the fault planes in each stress tensor inversion method. As mentioned above, the uncertainty of the principal stress axes was overlapping, and this indicates that the stress field does not significantly change. However, small differences in the stress field type may have affected the ST values.

The ST value differences between Michael's stress fields and the re-estimated stress fields using Vavryčuk's method

were within a range of 0.1 (Tables 5 and 8). The reversal of the ST values for the nodal planes (for example, "*Ts* of the east-dipping plane > *Ts* of the west-dipping plane" became "*Ts* of the east-dipping plane < *Ts* of the west-dipping plane") was not confirmed. The differences of 0.1 were mostly larger than the uncertainties for each result, and consequently, ST is likely to vary by 0.1 due to the small stress variations between the two methods. Thus, it is possible that a small change in the stress field may cause an error in the ST value of approximately 0.1.

Summary of the comparisons

The re-estimated stress fields determined using Vavryčuk's method had a smaller level of uncertainty and more stability than those estimated using Michael's method. However, the re-estimated stress fields were almost identical to those estimated using Michael's method. The small change in the results for the 2016 Oshika earthquake may be because of the differences in the selection of the fault planes in each stress tensor inversion method. The difference in selection is probably attributed to the small number of mechanism solutions. For the 2003 northern Miyagi earthquake, the stress fields estimated using Michael's method were sufficiently reliable.

Synthetic slip: rake difference vs. ST values

The rake angle (calculated rake) on the fault plane of the estimated stress field was calculated and then compared with the rake angle of the fault model (model rake). To calculate the rake, a synthetic slip program was utilized that was developed by Neves et al. (2009). To compare the calculated rake with the model rake, the following rake difference was defined:

$$Model\ rake - Calculated\ rake = Rake\ difference. \tag{6}$$

If the actual and estimated stress fields are similar, the rake differences are expected to be close to zero. The relationship between the model differences and ST was also examined. Rake differences are calculated using same dataset (local stress field and fault model) as the ST method.

Overall, the ST values were concentrated around 0.4–1.0 and rake differences around 0°–45° (Fig. 13). The 1998 Shizukuishi earthquake exhibited a rake difference of approximately 80° (Fig. 14). Earthquakes in the Tohoku inland area had larger rake differences than those in the EMJS area (Fig. 13). Moreover, even if the rake difference was the same on the east- and west-dipping planes, the east-dipping planes tended to show a higher ST value.

The Tohoku inland area was assessed in relation to three earthquakes (the 1998 Shizukuishi earthquake, 2003 northern Miyagi earthquake, and 2008 Iwate-Miyagi Nairiku earthquake). The whole term was divided into two terms: "term-I," before the 2011 Tohoku-Oki earthquake (blue dot in Fig. 14), and "term-II," after the 2011 Tohoku-Oki earthquake (red dot in Fig. 14). After the earthquake, the rake differences had a tendency to increase (red dot in Fig. 14) from < 20° to > 20° for the 2003 northern Miyagi earthquake and 2008 Iwate-Miyagi Nairiku earthquake. For the 1998 Shizukuishi earthquake, the rake differences were distributed around 20° for two of the four cases which used the term-I stress (blue dot in Fig. 14) but increased to 40°–90° for all four cases which used the term-II stress (red dot in Fig. 14). Therefore, if the stress field changed, the rake difference increased.

From the results of the stress field estimation in this study, the tendency of the stress fields was found to change before and after the 2011 Tohoku-Oki

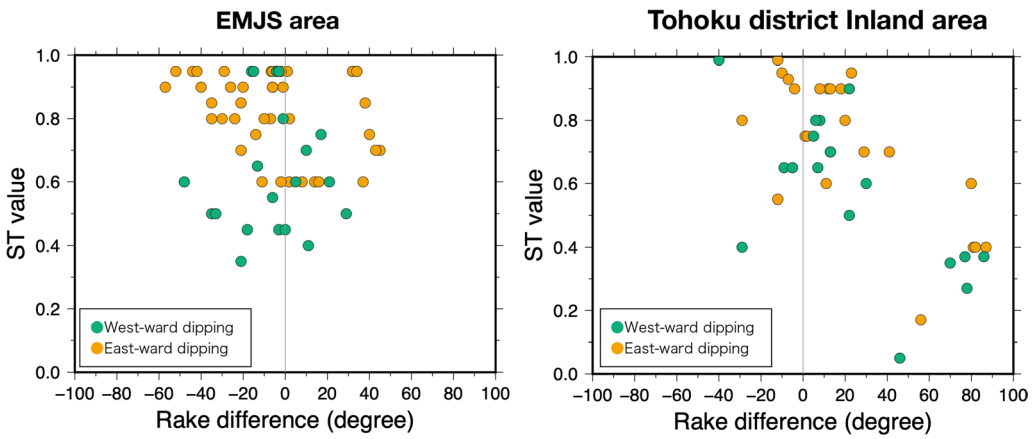

Fig. 13 Relationship between the rake difference and slip tendency (ST) values. Each dot indicates the rake difference and the ST values calculated for the target event in this study. Green dots denote the values for westward-dipping planes. Yellow dots denote the values of eastward-dipping planes

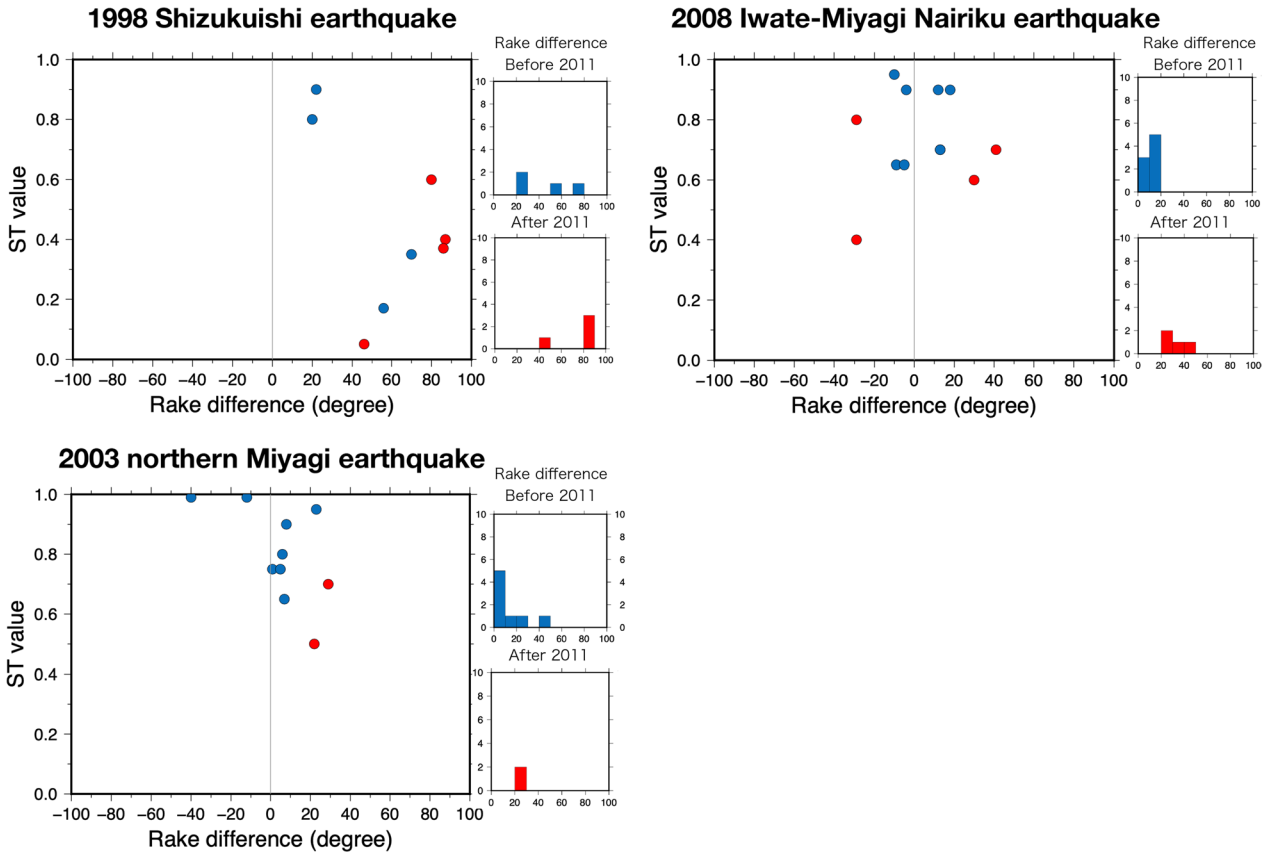

Fig. 14 Relationship between the rake difference and slip tendency (ST) values calculated for three inland events. Three events occurred in the Tohoku District inland area. Red and blue indicate data from before and after the Tohoku-Oki earthquake, respectively. A histogram showing the rake differences is shown

earthquake. This was attributed to the apparent change in the stress field caused by the stress change on the hanging wall side of the plate boundary (Okada et al. 2011, 2015; Yoshida et al. 2018). These changes in the stress field also affect the rake difference. For the 2008 Iwate-Miyagi Nairiku earthquake, blue dots in Fig. 14 show the results of the rake differences using the stress fields for term-I and term-II (time frame details were presented above in the Results, section). Consequently, all blue dots are distributed between the rake differences of 0° to 20°, and the ST values ranged from 0.6 to 1.0 (Fig. 14). The tendencies of the stress fields, ST values, and rake differences did not change before and after 2008.

These small rake differences imply that the stress field used for the calculation was closer to the state of the stress field when the event occurred. This indicates that it is better to use the stress field to evaluate the fault activities without the influence of the large earthquake (Tohoku-Oki earthquake).

Stress ratio change: influence of the 2011 Tohoku-Oki earthquake

Parameter setting in stress ratio change

In this study, the change in the stress field trend before and after the 2011 Tohoku-Oki earthquake was confirmed using the stress ratio change. The stress ratio change was determined to confirm if the changes in the stress fields were caused by the effects of the 2011 Tohoku-Oki earthquake using the fault model estimated in a previous study (Hayes 2011). The stress ratio change was calculated using the Coulomb program (Toda et al. 2005; Lin and Stein 2004). The friction coefficient in the fault gouge was estimated to be 0.1–0.2 (Lockner et al. 2011), while Byerlee (1978) estimated that it was 0.6 using experimental data. A simple calculation test was first conducted using the coefficient of friction $\mu = 0$, 0.1, 0.2, 0.3, 0.4, 0.5, and 0.6, and the results showed that when the coefficient of friction (μ) was 0.5 and 0.6 there was little change in the stress. Therefore, the coefficients of friction (μ) used were 0, 0.1, and 0.4. Hayes (2011) used a fault model of the Tohoku-Oki earthquake, where the

effective vertical stress was calculated from the lithostatic and hydrostatic pressures as follows:

$$\begin{aligned} &\textit{Effective vertical stress} = \textit{Lithostatic pressure} \\ &\quad - \textit{Hydrostatic pressure} \\ &= \left(2.84 \times 10^3 \times 9.8\right) Pa/m \\ &\quad - \left(1.00 \times 10^3 \times 9.8\right) Pa/m \sim 180 bar/km \end{aligned} \tag{7}$$

As a general values, rock density $= 2.84 \times 10^3 \mathrm{kg/m^3}$, water density $= 1.00 \times 10^3 \mathrm{kg/m^3}$, and acceleration of gravity $= 9.8 \mathrm{m/s^2}$. Therefore, the value of effective vertical stress was calculated to be 180 bar/km.

Based on this value, the minimum principal stress (S_3) for 180 bar/km and intermediate principal stress (S_2) for $S_3 \times 1.01, 1.02, 1.03, 1.04, 1.05, 1.06, 1.07, 1.08, 1.09, 1.10, 1.20, 1.30, 1.40,$ and$1.50,$ were evaluated. The maximum principal stress (S_1) was also calculated using the stress ratios S_2 and S_3. To consider the possibility that S_3 was smaller than 180 bar/km, we also calculated stress ratio change with S_3 for 45 bar/km (=quarter of 180 bar/km) and S_2 for $S_3 \times 1.01, \ldots, 1.50$. To investigate the results when changing the value of S_3, we examined with the S_2 instead of S_3 for 180 bar/km, 90 bar/km, and 45 bar/km and S_1 for $S_2 \times 1.01, \ldots, 1.50$.

The results of the stress fields estimated using Michael's method (input stress field) were used for the directions of the principal stress and stress ratio. In this section, three areas (the 1998 Shizukuishi earthquake, 2003 northern Miyagi earthquake, and 2008 Iwate-Miyagi Nairiku earthquake) are focused.

Results of stress ratio change

The stress ratio change was calculated from the focal mechanisms under the above conditions using the Coulomb program (Lin and Stein 2004; Toda et al. 2005). These focal mechanisms resulted in exhibiting stress fields. Michael's method was used to estimate the stress field (output stress field) using the output mechanism solution in the same area as that of the input stress field. In this study, we focus on the change in the stress ratio. The results of the output stress field were compared with the stress field estimated using the actual data. If the output stress field (result of stress ratio change) was similar to the stress field estimated using the actual data (stress field after 2011 Tohoku-Oki earthquake), this indicated a possibility that the stress change occurred due to the effects of the 2011 Tohoku-Oki earthquake under the same environment as we set.

Using this procedure, the conditions under which the stress field changes were examined, before and after the Tohoku-Oki earthquake, were thought to be the effects of the stress disturbances caused by large-scale earthquakes. All results showed similar types of stress fields and consequently, the stress ratio and the S_{Hmax} direction were focused on when comparing the stress fields.

The cases where the stress ratio and S_{Hmax} were closer to the stress fields after the Tohoku-Oki earthquake were confirmed, as described in the following.

1998 Shizukuishi earthquake In the case of the 1998 Shizukuishi earthquake, when S_3= 180 bar/km, the S_{Hmax} direction and stress ratio were closer to the stress field after the Tohoku-Oki earthquake and could not be reproduced by stress change (see Additional file 1: Fig. S1). When $S_3 = 45$ bar/km, S_2= 46.8 to 49.5 bar/km, S_1=81.0 to 135.0 bar/km and $\mu = 0$, the S_{Hmax} direction became close to the Tohoku-Oki earthquake (see Additional file 1: Fig. S2). When $S_3 = 45$ bar/km, S_2= 46.8 to 47.3 bar/km, S_1=81.0 to 90 bar/km and $\mu = 0.1$, the stress ratio became close to the Tohoku-Oki earthquake (see Additional file 1: Fig. S2).When $S_3 = 43.8$ bar/km, S_2= 45 bar/km, S_1= 67.5 bar/km, and $\mu = 0$, the S_{Hmax} direction became close to the Tohoku-Oki earthquake (see Additional file 1: Fig. S3). Furthermore, when S_3= 45.0 to 43.8 bar/km, S_2= 45 bar/km, and $\mu = 0.4$, S_{Hmax} the direction was smaller than that prior to the Tohoku-Oki earthquake (see Additional file 1: Fig. S3).

2003 northern Miyagi earthquake For the 2003 northern Miyagi earthquake, when S_3= 180 bar/km the S_{Hmax} direction was closer to that after the Tohoku-Oki earthquake in S_1 = 261.8 to 316.4 bar/km, S_2=234.0 to 270 bar/km, and $\mu = 0$ (see Additional file 1: Fig. S4). When S_3= 45 bar/km, S_1= 79.1 bar/km and S_2 =67.5 bar/km, the S_{Hmax} direction became closer to that after the Tohoku-Oki earthquake with $\mu = 0$, 0.1, and 0.4 (see Additional file 1: Fig. S5). Furthermore, the S_{Hmax} direction became closer to that after the Tohoku-Oki earthquake with the following three conditions: (1) S_2= 45 bar/km, S_1 = 49.5 to 67.5 bar/km, S_3 = 1.3 to 36.3 bar/km, and $\mu = 0.1$; (2) S_2= 45 bar/km, S_1 = 47.3 to 67.5 bar/km, S_3= 1.3 to 40.6 bar/km, and $\mu = 0$; and (3) S_2= 45 bar/km, S_1 = 47.7 to 67.5 bar/km, S_3= 1.3 to 39.8 bar/km, and μ= 0.4 (see Additional file 1: Fig. S6).

2008 Iwate-Miyagi Nairiku earthquake For the 2008 Iwate-Miyagi Nairiku earthquake, when S_3= 180 bar/km and $\mu = 0$, the S_{Hmax} direction and stress ratio became close to that after the Tohoku-Oki earthquake for S_1= 185.1 to 334.3 bar/km and S_2= 181.8 to 234.0 bar/km (see Additional file 1: Fig. S7). When S_3= 180 bar/km, the stress ratio became closer with the following three conditions: (1) S_1= 185.1 to 334.3 bar/km and S_2= 181.8 to 252.0 bar/km, and $\mu = 0$; (2) S_1= 282.9 to 334.3 bar/km and S_2= 216.0 to 252.0 bar/km, and $\mu = 0.1$; and (3) S_1= 205.7 to 334.3 bar/km and S_2= 189.0 to 252.0 bar/

km, and $\mu = 0.4$. When S_3= 45 bar/km, S_{Hmax} direction became similar with the following conditions: S_1= 46.3 to 47.6 bar/km, S_2= 45.5 to 45.9 bar/km, and $\mu = 0$, 0.1 and 0.4; S_1= 47.9 bar/km, S_2= 49.5 bar/km, and $\mu = 0$ and 0.1 (see Additional file 1: Fig. S8). When S_3= 45 bar/km, the stress ratio become similar with the S_1= 47.6, and 83.6 to 96.4 bar/km, S_2= 45.5, and 54.0 to 58.5 bar/km, and $\mu = 0$ (see Additional file 1: Fig. S8). Furthermore, when S_2= 180 bar/km and $\mu = 0$, S_{Hmax} the direction and stress ratio became closer after the Tohoku-Oki earthquake in S_1= 181.8 to 270.0 bar/km and S_3= 131.5 to 179.0 bar/km (see Additional file 1: Fig. S9). When S_2 = 180 bar/km and $\mu = 0.1$, S_{Hmax} the direction showed a smaller value than that prior to the Tohoku-Oki earthquake in S_1 = 181.8 to 216.0 bar/km and S_3= 131.5 to 160.6 bar/km. Furthermore, the stress ratio became close in S_1= 234.0 to 270.0 bar/km and S_3 = 150.9 to 131.5 bar/km. When S_2= 180 bar/km and $\mu = 0.4$, the stress ratio became closer to that after the Tohoku-Oki earthquake in S_1= 198.0 to 270.0 bar/km and S_3 = 131.5 to 170.3 bar/km.

Influence of the 2011 Tohoku-Oki earthquake on the stress field For the 1998 Shizukuishi and 2003 northern Miyagi earthquakes, the magnitude of S_3 was found to correspond to 30% of the lithostatic pressure, which might suggest a high pore fluid pressure of 70% of the lithostatic pressure, while for the 2008 Iwate-Miyagi Nairiku earthquake, the magnitude of S_3 corresponded to > 60% of the lithostatic pressure. This difference in the magnitude of S_3 may be due to the difference in decay time from the earthquakes, i.e., in the temporal recovery of fluid pressure (e.g., Sibson 1990).

Under some stress conditions we assumed a stress field similar to that observed after the Tohoku-Oki earthquake was confirmed. It is thus possible that the stress field changed after the Tohoku-Oki earthquake due to the stress disturbance caused by large-scale earthquakes under these conditions. Notably, this could be a possible interpretation; however, the temporal change was enhanced and apparently caused within the heterogeneous stress field and high pore fluid pressure (e.g., Smith and Dieterich 2010; Terakawa et al. 2013; Terakawa and Matsu'ura 2022). This result supports the idea that the factor of the large rake difference calculated using the stress field of the Tohoku-Oki earthquake (see above section) was caused by the effects of the Tohoku-Oki earthquake. The target events of this study, which are located in the Tohoku District inland area, occurred prior to the Tohoku-Oki earthquake. Thus, to evaluate the fault states under similar conditions when an event occurred, the stress field prior to the Tohoku-Oki earthquake should be used. In any case, the effects of the large earthquakes that caused changes in the stress field over a wide area should be excluded.

Comparison with previous studies

In this section, the results of this study are compared with those of relevant previous studies. Stress fields were estimated in this study, and the reverse fault type was found to be dominant in the EMJS. The S_{Hmax} direction was E–W in the northern area and rotated clockwise to the southern area. Furthermore, the S_{Hmax} direction was NW–SE in the Japan Sea area and rotated counterclockwise to the coastal area. The reverse fault type of stress field was dominant in the Tohoku District inland area. The S_{Hmax} direction was approximately E–W to WNW–ESE prior to the Tohoku-Oki earthquake. After the Tohoku-Oki earthquake, however, the S_{Hmax} direction was ENE–WSW to NE–SW in the northern area, while in the southern area, it was NW–SE.

The results of the stress fields in the Tohoku inland area were consistent with those of previous studies (e.g., Terakawa and Matsu'ura 2010; Miyakawa and Otsubo 2015; Yoshida et al. 2015; Yukutake et al. 2015; Miyakawa and Otsubo 2017; Terakawa and Matsu'ura 2022; Uchide et al. 2022). Terakawa and Matsu'ura (2010) estimated the stress fields in the EMJS area using fewer NIED moment tensor solutions than used in this study. Their results estimate the direction of maximum compression to be E–W in north of 39° N and WNW–ESE or NW–SE south of 39° N. Terakawa and Matsu'ura (2022) estimated centroid moment tensor data from 1997 to 2020 and confirmed that the stress direction prior to the 2011 Tohoku-Oki earthquake was stable for approximately 14 years. However, the stress direction changed after the 2011 Tohoku-Oki Earthquake. They concluded that the 2011 Tohoku-Oki earthquake caused these significant changes. Uchide et al. (2022) estimated the focal mechanism solution and stress field using data from NIED, Hinet, JMA (Japan Meteorological Agency), and GSJ/AIST (Geological Survey of Japan, AIST) stations. From their results, the S_{Hmax} showed an N–S direction along the Sanriku coast and an E–W direction in other areas of the Tohoku District. After the 2011 Tohoku-Oki earthquake, the S_{Hmax} direction was rotated clockwise and anticlockwise in the central and eastern parts of the Tohoku District area, respectively. Particularly in the southern part of the Tohoku District inland area, the direction of the shortening strain (e.g., Miura et al. 2004) and the results from this study for the S_{Hmax} direction were approximately the same. The detailed strain distribution in the northern part was unknown; however, the direction of the relative motion between the Amur Plate, corresponding to the western side of the EMJS area, and the North American

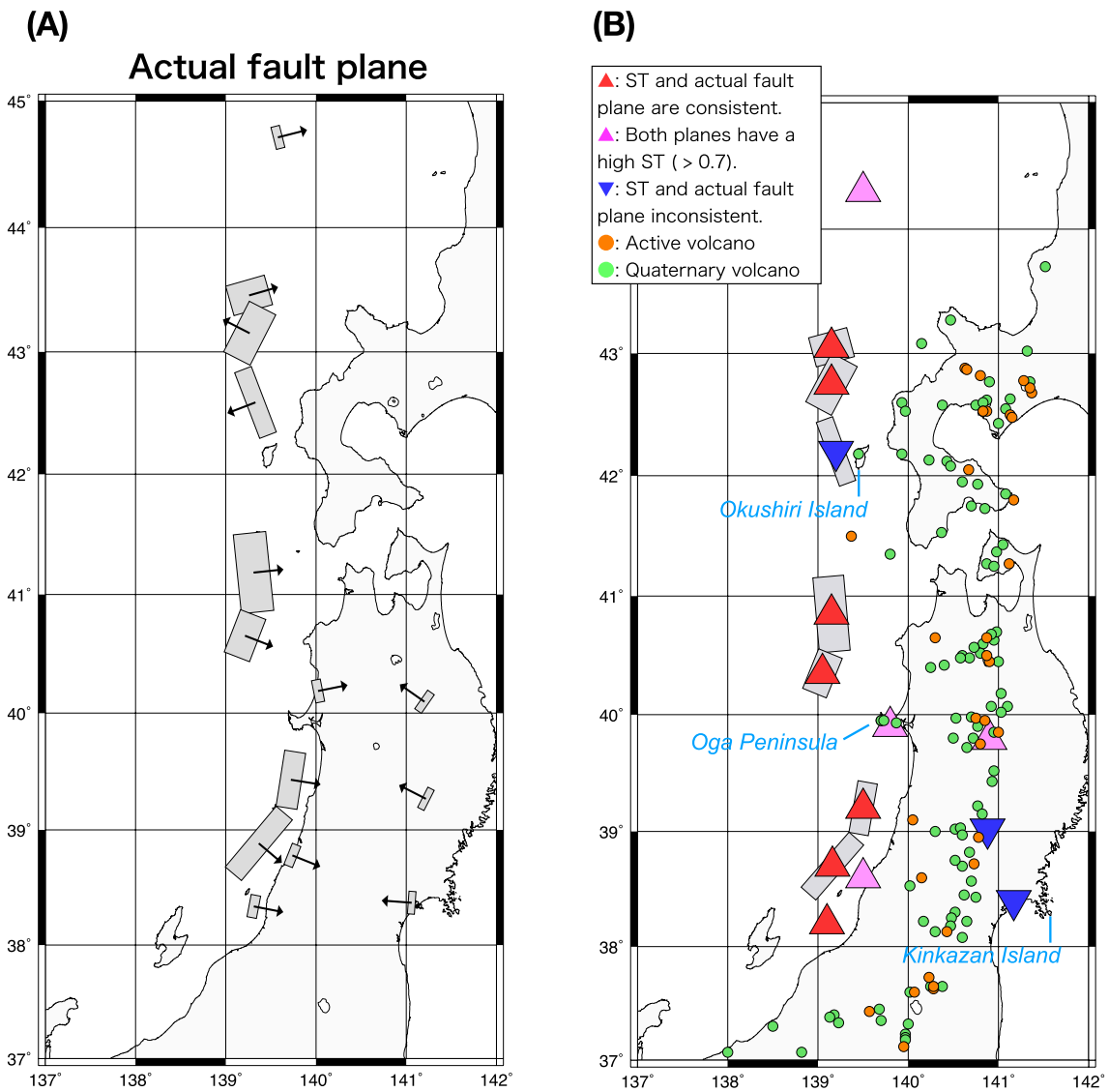

Fig. 15 Relationship between the actual fault planes and slip tendency (ST) values. **A** is same as **B** in Fig. 1. The arrow on the fault plane denotes the dipping direction. **B** The distribution of volcanoes and a summary of the relationship between the ST values and the actual fault plane in this study. Orange and green dots indicate the distributions of the active volcano and quaternary volcano, respectively. Red and blue triangles indicate the events for the actual fault plane, which has larger and smaller ST values, respectively. The pink triangle shows the events on both planes having a larger ST value

Plate (Heki et al. 1999) or Okhotsk Plate (Wei and Seno 1998), corresponding to the eastern side of the EMJS area, was estimated to be approximately E–W. This is consistent with the direction of maximum compression identified in the northern EMJS in this study.

The estimated ST values in the EMJS and Tohoku inland areas in this study were compared with the actual fault planes and ST values estimated in previous studies (e.g., Hatori 1969; Satake and Abe 1983; Aida 1984, 1989; Satake 1985, 1986; Umino et al. 1985, 1998; Kosuga et al. 1986; Sato et al. 1986; Nakanishi et al. 1993; Sato 1993; Tanioka et al. 1995; Okada et al. 2003, 2012; Ohta et al. 2008; Hurukawa and Harada 2013; Yoshida et al. 2014, 2016; Earthquake Research Committee 2019; Fig. 15). The low dip angle planes in this study showed high ST values ($Ts > 0.7$), and most of the fault planes were eastward-dipping. This means that fault planes with a low dip angle are favorable to slip in the study areas.

In the EMJS area, the fault planes that were thought to be active exhibited high ST values ($Ts > 0.7$). In contrast, in the Tohoku inland area, fault planes that actually slipped tended to have small ST values ($Ts < 0.6$).

Miyakawa and Otsubo (2015) discussed the effects of pore fluid pressure on the ST value. They assumed that pore fluid pressure affects the normal stress and calculated ST while varying the pressure. As a result, they examined the active fault with low ST values in the stress field of the Tohoku region (fault plane with a high dip angle), which revealed high ST values when the pore fluid pressure was high. Magma is one of the origins of underground pore water. Therefore, the volcanic distribution and ST values in Tohoku, Japan, were compared using a map for active volcanoes in Japan (https://www.data.jma.go.jp/svd/vois/data/tokyo/STOCK/bulletin/catalog/appendix/v_active.html) and list of Quaternary volcanoes (https://gbank.gsj.jp/volcano/index.htm).

The relationship between the distribution of volcanoes and the ST values determined in this study are shown in Fig. 15. In the Tohoku inland area, the results were selected using the stress field before the Tohoku-Oki earthquake. More volcanoes are distributed in the Tohoku inland area than in the EMJS area.

The 1998 Shizukuishi earthquake and 2008 Iwate-Miyagi Nairiku earthquake were characterized by the existence of volcanoes near the mainshocks. Additionally, around the 2003 northern Miyagi earthquake, low-seismic-velocity regions were distributed in the deeper regions, suggesting the existence of fluid (Okada et al. 2010). This suggests that high pore fluid pressure may be one of the factors that leads to the activation of high-west-dipping faults in the Tohoku inland area (e.g., Sibson 1990; Okada et al. 2007, 2012).

For the earthquakes around the Oshika Peninsula and Kinkazan Island, both nodal planes had almost the same dip angle (40°–50°) and calculated ST. As this area is in the east of the rift zone during the formation of the Japan Sea, it is possible that high-dip faults were not formed and that an earthquake occurred in the optimal newly formed fault plane for the present stress field.

In the EMJS area, the southern fault plane of the 1993 Hokkaido Nansei-oki earthquake exhibited low ST values. The southern plane was distributed on the western part of Okushiri Island. Mount Katsumayama is a Quaternary volcano located on Okushiri Island; therefore, high pore fluid pressure may have possibly affected its fault activity.

In contrast, the 1939 Oga earthquake occurred adjacent to the Quaternary volcanoes located in Oga Peninsula (Toga, Megata, and Kanpuz/;an). The Oga earthquake is presumed to have caused the activity of an east-dipping reverse fault extending N–S. Previous studies (e.g., Sato 1993) have suggested that an east-dipping plane with a low dip angle slipped during the Oga earthquake. Therefore, the ST values obtained in this study were relatively high for both planes.

Some studies have confirmed a low seismic wave velocity area, suggesting the existence of fluid in the Tohoku inland and EMJS areas (e.g., Zhao et al. 2011). However, the distribution of volcanoes suggested that the influence of the pore fluid pressure was greater in the Tohoku inland area than in the EMJS area. It was thus considered that the fault plane, which is unfavorable for slipping in the stress field, may be easily activated in the Tohoku inland area.

For the Oga earthquake, however, there were cases when west-dipping planes with a high dip angle were not active, even if volcanoes existed. This could be owing to one of the following three reasons: (1) there is no high-dip-angle fault plane; (2) the high-dip-angle fault plane has not been active for a long time and the cohesive force is recovering; or (3) the differential stress is small (Sibson 2012; Sibson and Ghisetti 2018, etc.). Comparisons between past seismic activity and future fault activity are thus necessary. Furthermore, examining the long-term activity is required to monitor the activity of old high-dip-angle fault planes in both the EMJS and Tohoku inland areas.

Conclusions

Stress fields in the Tohoku District of Japan, including the EMJS area, were estimated in this study. This was followed by an evaluation of the likelihood of fault slip using the ST method. The reliability of the stress fields was then examined by comparing the ST values with the actual activities. The following five conclusions were drawn:

1) The EMJS stress field has a reverse fault type that was also dominant in the Tohoku inland area. Prior to the 2011 Tohoku-Oki earthquake, the S_{Hmax} direction was from E–W to NW–SE; however, after the 2011 Tohoku-Oki earthquake, it changed from ENE–WSW to NE–SW. The stress change was calculated using a fault model for the Tohoku-Oki earthquake and the assumed effective vertical stress. Under the assumed conditions, the S_{Hmax} direction and stress ratio were examined and found to be similar to those of the stress field after the Tohoku-Oki earthquake. The stress change analysis showed that the stress disturbance from the 2011 Tohoku-Oki earthquake may have caused changes in the stress fields. The results thus indicate that when evaluating fault activity using stress fields, the effects of large earthquakes must also be considered.
2) The stress fields estimated using Michael's method showed a high level of uncertainty in the results for the 2003 northern Miyagi and 2016 Oshika Peninsula earthquakes. The stress fields were consequently re-estimated using the slip instability method, and the

results were more stable for the 2003 northern Miyagi earthquake and were altered for the 2016 Oshika Peninsula earthquake when compared to the results obtained using Michael's method. This is because the number of focal mechanism solutions was insufficient for the 2016 Oshika Peninsula earthquake. The results thus indicate that, to obtain more reliable results, an increased number of focal mechanisms is required. Furthermore, for the 2003 northern Miyagi earthquake, the magnitude correlation for the ST values was almost the same as with the Michael's and Vavryčuk's methods. If the stress differences are small, similar ST values could thus be obtained.

3) Rake differences were larger in the Tohoku inland area than in the EMJS area. The rake differences were larger after the 2011 Tohoku-Oki earthquake when compared with those before. The results of this and previous studies have confirmed that stress field trends changed before and after the 2011 Tohoku-Oki earthquake, although it is unclear whether this temporal change was actual or apparent in a heterogeneous stress field, such as in the aftershock area (e.g., Smith and Heaton 2015); however, the large rake may have influenced this change of direction. Thus, when a large earthquake causes a change in the stress field over a wide area, its effect should be excluded.
4) The ST values indicate that eastward-dipping planes with a low dip angle are favorable to slip under the stress field of the study area. In the EMJS area, eastward-dipping fault planes with low dip angles exhibited large ST values, which is consistent with the actual fault activity. In the EMJS, fault slipping is favorable with the current stress field. In the Tohoku inland area, the eastward-dipping fault plane showed a large ST value; however, the actual fault plane estimated in previous studies was westward-dipping and had a high dip angle. The results indicate that the actual fault plane is unlikely to slip with the current stress field in the Tohoku inland area.
5) Fault planes that cannot easily slip into stress fields, such as the fault plane in the Tohoku inland area and the southern part of the fault model of 1993 Hokkaido Nansei-oki earthquake, are favorable in volcano neighborhoods. Factors related to volcanic activity (e.g., pore fluid pressure) may thus cause fault activity.
6) Overall, the study shows that the ST value does not change significantly when the estimated stress field is stable in the Tohoku inland area, where the slipping of planes into the stress field is unfavorable, and consequently, certain factors and other stress fields were identified as causing fault slip.

To identify the factors that cause fault slip, similar evaluations of other cases from different regions will be required. Furthermore, to include values such as the pore fluid pressure and friction coefficient in the ST value, it will be necessary to confirm the factors that cause slip.

Abbreviations

EMJS	Eastern margin of the Japan Sea
I	Fault instability
MTRF	Moment tensor rate functions
S_1 or σ_1	Maximum principal stress
S_2 or σ_2	Intermediate principal stress
S_3 or σ_3	Minimum principal stress
S_{Hmax}	Maximum horizontal direction
ϕ	Stress ratio
SC	Stress change
SF	Stress field
ST	Slip tendency
μ	Friction coefficient

Supplementary Information

The online version contains supplementary material available at https://doi.org/10.1186/s40623-024-01986-w.

Additional file 1. Supporting information, figures and tables. The results of an additional analysis of the ST method and stress ratio change are showed in this file.

Acknowledgements
This study used data provided by the Group for the aftershock observations of the 2011 off the Pacific coast of Tohoku Earthquake. The group members were the authors and coauthors of Okada et al. (2015). We would like to thank Editage (www.editage.com) for English language editing.

Author contributions
AT: conceptualization, data curation, formal analysis, investigation, methodology, visualization, and writing the original draft. MM: conceptualization, writing—review & editing. TO: supervision, writing—review and editing. SS: data curation, writing—review and editing. MO: data curation, writing—review & editing. KK: data curation, writing—review and editing. MK: data curation, writing—review & editing. YY: data curation, writing—review and editing. HK: data curation, writing—review and editing. TMs: data curation, writing—review and editing. HY: data curation, writing—review and editing. SHi: data curation, writing—review and editing. TK: data curation, writing—review and editing. SHo: data curation, writing—review and editing. TMz: supervision, writing—review and editing. SK: review and editing. TN: review and editing. Group for the aftershock observations of the 2011 off the Pacific coast of Tohoku Earthquake: data provision. All authors have read and approved the final manuscript.

Funding
This work was supported by The International Joint Graduate Program in Earth and Environmental Sciences, Tohoku University (GP-EES) and the Pioneering Research Program for Next Generation Researchers of the JST (JST SPRING, Grant Number JPMJSP2114).

Availability of data and materials
All data and materials are available from the corresponding author upon request.

Declarations

Ethics approval and consent to participate
Not applicable.

Consent for publication
Not applicable.

Competing interests
The authors have no competing interests to declare.

Author details
[1]Research Center for Prediction of Earthquakes and Volcanic Eruptions, Graduate School of Science, Tohoku University, 6-6 Aza-Aoba, Aramaki, Aoba-Ku, Sendai 980-8578, Japan. [2]Earthquake Research Institute, University of Tokyo, 1-1-1 Yayoi, Bunkyo-Ku, Tokyo 113-0032, Japan. [3]Institute of Seismology and Volcanology, Faculty of Science, Hokkaido University, Kita-10 Nishi-8, Kita-Ku, Sapporo 060-0810, Japan. [4]Graduate School of Science and Technology, Hirosaki University, 3, Bunkyo-Cho, Hirosaki 036-8561, Japan. [5]Graduate School of Environmental Studies, Nagoya University, D2-1 (510) Furo-Cho, Chikusa-Ku, Nagoya 464-8601, Japan. [6]Research Center for Earthquake Prediction, Disaster Prevention Research Institute, Kyoto University, Gokasho, Uji 611-011, Japan. [7]Institute of Seismology and Volcanology, Faculty of Science, Kyushu University, 2-5643-29 Shin'yama, Shimabara 855-0843, Japan. [8]Nansei-Toko Observatory for Earthquakes and Volcanoes, Kagoshima University, 1-21-40 Korimoto, Kagoshima 890-0065, Japan. [9]Facilities Division, School of Engineering, Tohoku University, Tohoku University, 6-6 Aza-Aoba, Aramaki, Aoba-Ku, Sendai 980-8578, Japan.

Received: 6 July 2023 Accepted: 21 February 2024
Published online: 07 March 2024

References

Aida Y (1984) A source model of the tsunami accompanying the 1983 Nihonkai-Chubu earthquake. Bull Earthq Res Ins Uni Tokyo 59(1):93–104
Aida Y (1989) Numerical simulation for the tsunami associated with the Shonai-Oki earthquake of the 4th year of Tempou. Pal-Earthq Seq Vol Truth Fict Images 204–214.
Byerlee J (1978) Friction of rocks. Pure Apply Geophys 116:615–626. https://doi.org/10.1007/BF00876528
Collettini C, Trippetta F (2007) A slip tendency analysis to test mechanical and structural control on aftershock rupture planes. Earth Planet Sci Lett 255(3–4):402–413. https://doi.org/10.1016/j.epsl.2007.01.001
Earthquake Research Committee (2003) Long-term evaluation of seismic activity in the eastern margin of the Japan Sea. https://www.jishin.go.jp/main/chousa/03jun_nihonkai/index.html. Accessed 5th Apr 2023.
Earthquake Research Committee (2019) Evaluation of the june 18th, 2019, Yamagata-Oki earthquake. https://www.jishin.go.jp/main/oshirase/20190618_yamagata.html. Accessed 5th Apr 2023
Fukao Y, Furumoto M (1975) Mechanism of large earthquakes along the eastern margin of the Japan sea. Tectonophysics 26(3–4):247–266. https://doi.org/10.1016/0040-1951(75)90093-1
Fukuyama E, Ishida S, Dreger DS, Kawai H (1998) Automated seismic moment tensor determination by using on-line broadband seismic waveforms. Zisin Ser 51:149–156. https://doi.org/10.4294/zisin1948.51.1_149
Hardebeck JL, Shearer PM (2002) A new method for determining first-motion focal mechanisms. Bull Seis Soc Amer 92:2264–2276. https://doi.org/10.1785/0120010200
Hatori T (1969) A study of the wave source of tsunami generated off West Hokkaido on Aug. 2, 1940. Bull Earthq Res Inst Uni Tokyo 47(6):1063–1072
Hayes GP (2011) Rapid source characterization of the 2011 M_w 9.0 off the Pacific coast of Tohoku earthquake. Earth Planets Space 63:529–534. https://doi.org/10.5047/eps.2011.05.012
Heki K, Miyazaki S, Takahashi H, Kasahara M, Kimata F, Miura S, Vasilenko NF, Ivashchenko A, An KD (1999) The Amurian Plate motion and current plate kinematics in eastern Asia. J Geophys Res Solid Earth 104:29147–29155. https://doi.org/10.1029/1999JB900295
Hirasawa T (1965) Source mechanism of the Niigata earthquake of June 16, 1964, as derived from body waves. J Phys Earth 13:35–66. https://doi.org/10.4294/jpe1952.13.35
Hurukawa N, Harada T (2013) Fault plane of the 1964 Niigata earthquake, Japan, derived from relocation of the mainshock and aftershocks by using the modified joint hypocenter determination and grid search methods. Earth Planets Space 65:1441–1447. https://doi.org/10.5047/eps.2013.06.007
Jolivet L, Tamaki K, Fournier M (1994) Japan sea, opening history and mechanism: a synthesis. J Geophys Res Solid Earth 99:22237–22259. https://doi.org/10.1029/93JB03463
Kobayashi Y (1983) Initiation of "subduction" of plates. Chikyu 5:510–518
Kosuga M, Ikeda H, Kamazuka Y, Sato H (1986) Static fault model of the 1983 Nihonkai-Chubu (Japan Sea) earthquake as inferred from aftershock distribution crustal deformation, and tsunami data. J Geod Soc Jpn. 32:290–302. https://doi.org/10.11366/sokuchi1954.32.290
Lin J, Stein RS (2004) Stress triggering in thrust and subduction earthquakes and stress interaction between the southern San Andreas and nearby thrust and strike-slip faults. J Geophys Res Solid Earth. https://doi.org/10.1029/2003JB002607
Lockner DA, Morrow C, Moore D, Hickman S (2011) Low strength of deep San Andreas fault gouge from SAFOD core. Nature 472:82–85. https://doi.org/10.1038/nature09927
Lund B, Slunga R (1999) Stress tensor inversion using detailed microearthquake information and stability constraints: application to Ölfus in southwest Iceland. J Geophys Res Solid Earth 104:14947–14964. https://doi.org/10.1029/1999JB900111
Michael AJ (1984) Determination of stress from slip data: faults and folds. J Geophys Res Solid Earth 89:11517–11526. https://doi.org/10.1029/JB089iB13p11517
Michael AJ (1987) Use of focal mechanisms to determine stress: a control study. J Geophys Res Solid Earth 92:357–368. https://doi.org/10.1029/JB092iB01p00357
Miura S, Sato T, Hasegawa A, Suwa Y, Tachibana K, Yui S (2004) Strain concentration zone along the volcanic front derived by GPS observations in NE Japan arc. Earth Planets Space 56:1347–1355. https://doi.org/10.1186/BF03353360
Miyakawa A, Otsubo M (2015) Applicability of slip tendency for understanding long-term fault activity: a case study of active faults in northeastern Japan. J Jpn Soc Civil Eng 3:105–114. https://doi.org/10.2208/journalofjsce.3.1_105
Miyakawa A, Otsubo M (2017) Evolution of crustal deformation in the northeast-central Japanese island arc: Insights from fault activity. Isla Arc 26:e12179. https://doi.org/10.1111/iar.12179
Moeck I, Kwiatek G, Zimmermann G (2009) Slip tendency analysis, fault reactivation potential and induced seismicity in a deep geothermal reservoir. J Struct Geol 31:1174–1182. https://doi.org/10.1016/j.jsg.2009.06.012
Morris A, Ferril DA, Henderson DB (1996) Slip-tendency analysis and fault reactivation. Geology 24:275–278. https://doi.org/10.1130/0091-7613(1996)024%3c0275:STAAFR%3e2.3.CO;2
Nakanishi I, Kodaira S, Kobayashi R, Kikuchi M, Kasahara M (1993) The 1993 Japan Sea earthquake: Quake and tsunamis devastate small town. EOS Trans 74:377–379. https://doi.org/10.1029/93EO00599
Neves MC, Paiva LT, Luis J (2009) Software for slip-tendency analysis in 3D: a plug-in for Coulomb. Comp Geosci 35:2345–2352. https://doi.org/10.1016/j.cageo.2009.03.008
Ohta Y, Ohzono M, Miura S, Iinuma T, Tachibana K, Takatsuka K, Miyao K, Sato T, Umino N (2008) Coseismic fault model of the 2008 Iwate-Miyagi Nairiku earthquake deduced by a dense GPS network. Earth Planets Space 60:1197–1201. https://doi.org/10.1186/BF03352878
Okada T, Umino N, Hasegawa A (2003) Rupture process of the July 2003 northern Miyagi earthquake sequence, NE Japan, estimated from double-difference hypocenter locations. Earth Planets Space 55:741–750. https://doi.org/10.1186/BF03352483
Okada T, Hasegawa A, Suganomata J, Umino N, Zhang H, Thurber CH (2007) Imaging the heterogeneous source area of the 2003 M6.4 northern Miyagi earthquake, NE Japan, by double-difference tomography. Tectonophysics 430:67–81. https://doi.org/10.1016/j.tecto.2006.11.001
Okada T, Umino N, Hasegawa A (2010) Deep structure of the Ou mountain range strain concentration zone and the focal area of the 2008 Iwate-Miyagi Nairiku earthquake, NE Japan—seismogenesis related with magma and crustal fluid. Earth Planets Space 62:347–352. https://doi.org/10.5047/eps.2009.11.005
Okada T, Yoshida K, Ueki S, Nakajima J, Uchida N, Matsuzawa T, Umino N, Hasegawa A (2011) Shallow inland earthquakes in NE Japan possibly

triggered by the 2011 off the Pacific coast of Tohoku earthquake. Earth Planets Space 63:749–754. https://doi.org/10.5047/eps.2011.06.027
Okada T, Umino N, Hasegawa A (2012) Hypocenter distribution and heterogeneous seismic velocity structure in and around the focal area of the 2008 Iwate-Miyagi Nairiku earthquake, NE Japan—possible seismological evidence for a fluid driven compressional inversion earthquake. Earth Planets Space 64:717–728. https://doi.org/10.5047/eps.2012.03.005
Okada T, Matsuzawa T, Umino N, Yoshida K, Hasegawa A, Takahashi H, Yamada T, Kosuga M, Takeda T, Kato A, Igarashi T, Obara K, Sakai S, Saiga A, Iidaka T, Iwasaki T, Hirata N, Tsumura N, Yamanaka Y, Terakawa T, Nakamichi H, Okuda T, Horikawa S, Katao H, Miura T, Kubo A, Matsushima T, Goto K, Miyamachi H (2015) Hypocenter migration and crustal seismic velocity distribution observed for the inland earthquake swarms induced by the 2011 Tohoku-Oki earthquake in NE Japan: implications for crustal fluid distribution and crustal permeability. Crustal Permeability 15:307–323. https://doi.org/10.1111/gfl.12112
Okada T, Nakayama T, Hirahara S, Tateiwa K, Hirouchi S, Katsumata K, Ohzono M, Kosuga M, Maeda T, Yamanaka Y, Katao H, Matsuchima T, Yakiwara H, Group for the aftershock observation of the 2011 off the Pacific coast of Tohoku earthquake (2022) Temporal seismic observation in the central-southern part of Tohoku district. Toh J Nat Dis Sci 55:19–24
Okamura Y (2010) Relationships between geological structure and earthquake source faults along the eastern margin of the Japan Sea. J Geol Soc Jpn 116:582–591. https://doi.org/10.5575/geosoc.116.582
Okamura Y, Kato Y (2002) Tectonic landform and active fault in ocean area. Active faults and seismo-tectonics of the eastern margin of the Japan sea. University of Tokyo Press, Tokyo, pp 47–69
Okamura Y, Kuramoto S, Satoh M (1998) Active structures and their relation to earthquakes along the eastern margin of the Japan Sea. Bull Geol Surv Jpn 49:1–18
Satake K (1985) The mechanism of the 1983 Japan Sea earthquake as inferred from long-period surface waves and tsunamis. Phys Earth Planet Inter 37:249–260. https://doi.org/10.1016/0031-9201(85)90012-3
Satake K (1986) Re-examination of the 1940 Shakotan-oki earthquake and the fault parameters of the earthquakes along the eastern margin of the Japan Sea. Phys Earth Planet Inter 43:137–147. https://doi.org/10.1016/0031-9201(86)90081-6
Satake K, Abe K (1983) A fault model for the NIIGATA, JAPAN, earthquake of June 16, 1964. J Phys Earth 31:217–223. https://doi.org/10.4294/jpe1952.31.217
Sato H (1993) Reexamination of the 1939 Oga earthquake through the associated crustal movement. J Seis Soc Jpn 46:49–52. https://doi.org/10.4294/zisin1948.46.1_49
Sato H (1994) The relationship between Late Cenozoic tectonic events and stress field and basin development in northeast Japan. J Geophys Res Solid Earth 99:22261–22274. https://doi.org/10.1029/94JB00854
Sato T, Kosuga K, Tanaka K (1986) Aftershock distribution of the 1983 Nihonkai-Chubu (Japan Sea) earthquake determined from relocated hypocenters. J Phys Earth 34:203–223. https://doi.org/10.4294/jpe1952.34.203
Scholz CH (1988) The brittle-plastic transition and the depth of seismic faulting. Geol Rundsch 77:319–328. https://doi.org/10.1007/BF01848693
Sibson RH (1990) Rupture nucleation on unfavorably oriented faults. Bull Seismol Soc Am 80:1580–1604
Sibson RH (2009) Rupturing in overpressured crust during compressional inversion—the case from NE Honshu, Japan. Tectonophysics 473:404–416. https://doi.org/10.1016/j.tecto.2009.03.016
Sibson RH (2012) Reverse fault rupturing: competition between non-optimal and optimal fault orientations. Geol Soc Spec Publ 367:39–50. https://doi.org/10.1144/SP367.4
Sibson RH, Ghisetti FC (2018) Review: factors affecting the assessment of earthquake hazard from compressional inversion structure. Bull Seismol Soc Am 108:1819–1836. https://doi.org/10.1785/0120170375
Smith DE, Dieterich JH (2010) Aftershock sequences modeled with 3-d stress heterogeneity and rate-state seismicity equations: implications for crustal stress estimation. Pure Apply Geophys 167:1067–1085. https://doi.org/10.1007/s00024-010-0093-1
Smith DE, Heaton TH (2015) Reply to "comment on 'models of stochastic, spatially varying stress in the crust compatible with focal-mechanism data, and how stress inversions can be biased toward the stress rate' by Deborah Elaine Smith and Thomas H. Heaton" by Jeanne L. Hardebeck Bull Seismol Soc Am 105:1396–1421. https://doi.org/10.1785/0120100058
Taira A (2001) Tectonic evolution of the Japanese island arc system. Ann Rev Earth Planet Sci 29:109–134. https://doi.org/10.1146/annurev.earth.29.1.109
Tanioka Y, Satake K, Ruff L (1995) Total analysis of the 1993 Hokkaido Nansei-oki earthquake using seismic wave, tsunami, and geodetic data. Geophys Res Lett 22:9–12. https://doi.org/10.1029/94GL02787
Terakawa T, Matsu'ura M (2010) The 3-D tectonic stress fields in and around Japan inverted from centroid moment tensor data of seismic events. Tectonophysics 26(6):29(TC6008). https://doi.org/10.1029/2009TC002626
Terakawa T, Matsu'ura M (2023) Tectonic stress fields inferred from long-term CMT data ranging over different periods. Geophys J Intern 233:162–181. https://doi.org/10.1093/gji/ggac449
Terakawa T, Hashimoto C, Matsu'ura M (2013) Changes in seismic activity following the 2011 Tohoku-oki earthquake: effects of pore fluid pressure. Earth Planet Sci Lett 365:17–24. https://doi.org/10.1016/j.epsl.2013.01.017
Toda S, Stein RS, Richards-Dinger K, Bozkurt S (2005) Forecasting the evolution of seismicity in southern California: animations built on earthquake stress transfer. J Geophys Res Solid Earth. https://doi.org/10.1029/2004JB003415
Uchide T, Shiina T, Imanishi K (2022) Stress map of Japan: Detailed nationwide crustal stress field inferred from focal mechanism solutions of numerous microearthquakes. J Geophys Res Solid Earth 127:e2022JB024036. https://doi.org/10.1029/2022JB024036
Umino N, Hasegawa A, Obara K, Matsuzawa T, Shimizu H, Takagi A, Tanaka K, Kosuga M (1985) Hypocenter distribution of foreshocks and aftershocks of the 1983 Japan Sea earthquake. J Seis Soc Jpn 38:399–410. https://doi.org/10.4294/zisin1948.38.3_399
Umino N, Okada T, Nakamura A, Nakajima J, Sato T, Hori S, Kono T, Nida K, Ueki S, Matsuzawa T, Hasegawa A, Hamaguchi H (1998) Aftershock distribution for the M6.1 earthquake of 3 September 1998 in Shizukuishi, Iwate prefecture, northeastern Japan. Active Fault Res 17:1–8. https://doi.org/10.11462/afr1985.1998.17_1
Vavryčuk V (2014) Iterative joint inversion for stress and fault orientations from focal mechanisms. Geophys J Inter 199:69–77. https://doi.org/10.1093/gji/ggu224
Vavryčuk V, Bouchaala F, Fischer T (2013) High-resolution fault image from accurate locations and focal mechanisms of the 2008 swarm earthquakes in West Bohemia. Czech Republic Tectonophysics 590:189195. https://doi.org/10.1016/j.tecto.2013.01.025
Wei D, Seno T (1998) Determination of the Amurian plate motion. In mantle dynamics and plate interactions in East Asia. Mantle Dyn Plate Interac East Asia 27:337–346. https://doi.org/10.1029/GD027p0337
Yoshida K, Hasegawa A, Okada T, Iinuma T (2014) Changes in the stress field after the 2008 M7.2 Iwate-Miyagi Nairiku earthquake in northeastern Japan. J Geophys Res Solid Earth 119:9016–9030. https://doi.org/10.1002/2014JB011291
Yoshida K, Hasegawa A, Okada T (2015) Spatial variation of stress orientations in NE Japan revealed by dense seismic observations. Tectonophysics 647–648:63–72. https://doi.org/10.1016/j.tecto.2015.02.013
Yoshida K, Hasegawa A, Okada T (2016) Heterogeneous stress field in the source area of the 2003 M6.4 Northern Miyagi prefecture, NE Japan, earthquake. Geophy J Inter 206:408–419. https://doi.org/10.1093/gji/ggw160
Yoshida K, Hasegawa A, Yoshida T, Matsuzawa T (2018) Heterogeneities in stress and strength in Tohoku and its relationship with earthquake sequences triggered by the 2011 M9 Tohoku-Oki Earthquake. Pure Apply Geophys 176:1335–1355. https://doi.org/10.1007/s00024-018-2073-9
Yukutake Y, Takeda T, Yoshida A (2015) The applicability of frictional reactivation theory to active faults in Japan based on slip tendency analysis. Earth Planet Sci Lett 411:188–198. https://doi.org/10.1016/j.epsl.2014.12.005
Zhao D, Huang Z, Umino N, Hasegawa A, Yoshida T (2011) Seismic imaging of the Amur-Okhotsk plate boundary zone in the Japan Sea. Phys Earth Planet Inter 188:82–95. https://doi.org/10.1016/j.pepi.2011.06.013

Publisher's Note

Ayaka Tagami Graduate student in Graduate School of Science, Tohoku University.

Miu Matsuno Graduate student in Graduate School of Science, Tohoku University.

Tomomi Okada Associate Professor in Research Center for Prediction of Earthquakes and Volcanic Eruptions, Graduate School of Science, Tohoku University.

Shin'ichi Sakai Professor in Earthquake Research Institute, University of Tokyo.

Mako Ohzono Associate Professor in Institute of Seismology and Volcanology, Faculty of Science, Hokkaido University.

Kei Katsumata Associate Professor in Institute of Seismology and Volcanology, Faculty of Science, Hokkaido University.

Masahiro Kosuga Professor Emeritus in Graduate School of Science and Technology, Hirosaki University.

Yoshiko Yamanaka Associate professor in Graduate School of Environmental Studies, Nagoya University.

Hiroshi Katao Associate Professor in Research Center for Earthquake Prediction, Disaster Prevention Research Institute, Kyoto University.

Takeshi Matsushima Professor in Institute of Seismology and Volcanology, Faculty of Science, Kyushu University.

Hiroshi Yakiwara Associate Professor in Nansei-toko Observatory for Earthquakes and Volcanoes, Kagoshima University.

Satoshi Hirahara Technical staff member of Research Center for Prediction of Earthquakes and Volcanic Eruptions, Graduate School of Science, Tohoku University.

Toshio Kono Technical staff member of Research Center for Prediction of Earthquakes and Volcanic Eruptions, Graduate School of Science, Tohoku University.

Shu'ichiro Hori Technical staff member of Research Center for Prediction of Earthquakes and Volcanic Eruptions, Graduate School of Science, Tohoku University.

Toru Matsuzawa Professor in Research Center for Prediction of Earthquakes and Volcanic Eruptions, Graduate School of Science, Tohoku University.

Shuutoku Kimura Technical staff member of Research Center for Prediction of Earthquakes and Volcanic Eruptions, Graduate School of Science, Tohoku University.

Takashi Nakayama Technical staff member of Facilities Division, School of Engineering, Tohoku University.